



Designed Assembly and Integration of Colloidal Nanocrystals for Device Applications

liwoong Yang, Moon Kee Choi, Dae-Hyeong Kim,* and Taeghwan Hyeon*

Colloidal nanocrystals have been intensively studied over the past three decades due to their unique properties that originate, in large part, from their nanometer-scale sizes. For applications in electronic and optoelectronic devices, colloidal nanoparticles are generally employed as assembled nanocrystal solids, rather than as individual particles. Consequently, tailoring 2D patterns as well as 3D architectures of assembled nanocrystals is critical for their various applications to micro- and nanoscale devices. Here, recent advances in the designed assembly, film fabrication, and printing/integration methods for colloidal nanocrystals are presented. The advantages and drawbacks of these methods are compared, and various device applications of assembled/integrated colloidal nanocrystal solids are discussed.

1. Introduction

Over the past three decades, research on colloidal nanocrystals (NCs) has been intensively pursued due to their unique material properties and various related applications. [1-7] Because of their nanometer scale, many of the physical and chemical properties of NCs are strongly dependent on their sizes and shapes, which impart novel characteristics, such as the quantumconfinement effect of semiconductor NCs (i.e., quantum dots (QDs)),[8,9] the superparamagnetism of magnetic NCs,[10,11] the surface plasmon resonance in noble-metal nanoparticles (NPs),[12,13] and a giant Zeeman splitting in magnetic doped semiconductor NCs.[14,15] Consequently, extensive research has been conducted on the synthesis of monodisperse NCs of various materials with controlled particle sizes and shapes.^[16] Through these designed "wet" chemical synthetic approaches, highly monodisperse NCs with sizes from 1 nm to the tens of nm range have been successfully synthesized. Materials comprising these chemically synthesized NCs include metals,[17-19] semiconductors, [20-24] and metal oxides. [25-28]

In parallel with the advances in NC chemical synthesis, various integration and assembly techniques have been developed to fabricate nano-/microstructures for applications in

J. Yang, M. K. Choi, Prof. D.-H. Kim, Prof. T. Hyeon Center for Nanoparticle Research Institute for Basic Science (IBS) Seoul 151-742, Republic of Korea E-mail: dkim98@snu.ac.kr; thyeon@snu.ac.kr

J. Yang, M. K. Choi, Prof. D.-H. Kim, Prof. T. Hyeon School of Chemical and Biological Engineering Seoul National University Seoul 151-742, Republic of Korea

DOI: 10.1002/adma.201502851



electronic and optoelectronic devices.[29-34] In addition to the novel size- and shapedependent properties observed in individual NCs, the designed assembly of NCs provides a simple approach for generating "NC solid" ensembles with unique properties that are different from discrete NCs and/or bulk materials.[35] Numerous 2D and3D structures based on assembled NC solids have been fabricated. As NCs are "free standing" in their as-synthesized state, post-chemical assembly processes and thin-film fabrication techniques can integrate NCs in desired configurations for various device applications, which cannot be attained for epitaxially grown

films. These nanoarchitectures based on assembled NC solids can replace various elements of conventional devices while creating novel functions or performances based on the unique properties of the NCs. For example, metal NPs have been used as electrodes or photoamplification materials, whereas semiconducting QDs have been employed as active materials in light-emitting diodes (LEDs) or solar cells. [29,31,32] Furthermore, metal-oxide NCs have been actively investigated as light-trapping or electron-transporting materials in solar cells.[5,29,31]

In these device applications, generally, NCs are vertically stacked in a variety of organic/inorganic layers in the form of patterned films/layers. Therefore, the controlled formation and stacking of patterned NC films with uniform thickness and low roughness on diverse materials/substrates is very important. For many of these device applications, NC solids must have elaborate patterns with well-defined positions to be integrated into one consolidated system from individually separated device units. For example, to fabricate a full-color QD LED (QLED) array, several different kinds of QDs (e.g., red, green, and blue QDs) in tens of nanometer thicknesses and various patterns must be aligned on a single substrate without crosscontaminations.^[32] Therefore, various thin-film fabrication methods, including casting, dip coating, Langmuir-Blodgett (LB) deposition, and doctor blading, have been explored for the assembly of NCs. Patterns with greater complexity can be formed through printing techniques such as screen printing, inkjet printing, 3D printing, and transfer printing. The controlled shape, thickness, resolution, and layout of the NC solids maximize the benefits of the nanomaterials in specific applications. For future industrial production, the economical factors of each process also should be considered.

Here, we address recent advances in various film-fabrication, assembly, and printing/integration methods for colloidal NCs. The aim of this work is to guide readers in multidisciplinary

ADVANCED MATERIALS

www.advmat.de

www.MaterialsViews.com

research areas through the available techniques that have been commonly used for colloidal NCs. Elaborateness, uniformity, reproducibility, production yield, and scalability are important parameters to judge the techniques (**Figure 1**). The advantages and limitations of these processes are compared, and finally, the various device applications of assembled/integrated colloidal NC solids are reviewed. Nowadays, in particular, NC layers are diversely and intensively employed in electronics (conductors, transistors, memory), ^[5] optoelectronics (LEDs, solar cells, photodetectors), ^[31,32] electrochemical devices (batteries, smart windows), ^[36,37] and photoelectrochemical devices (solar-to-fuel cells). ^[38,39] Among these, special focus is on electronic/optoelectronics devices.

2. Film Fabrication using NC Building Blocks

In electronic and optoelectronic device applications, colloidal NCs are typically integrated in the form of NC solids (generally, thin films composed of colloidal NCs). Thus, an efficient process for the preparation of high-quality patterned films made up of colloidal NCs is an important requirement for fabricating these devices. Solution processes have been widely used for NC film fabrication, because as-synthesized colloidal NCs are dispersed in organic solvents and various polymeric and organic electronic materials are involved during the fabrication process. Furthermore, these solution processes are generally less expensive than conventional vacuum techniques. In this section, we present review of various fabrication methods that have been used for colloidal NC solids and NC superlattices. The representative characteristics of each method are compared and summarized in Table 1.

2.1. Colloidal Nanocrystals

Colloidal synthetic methods offer facile routes to tailor the size and shape of NCs, which cannot be achieved by typical top-down fabrication processes. By varying the design/reaction parameters, the characteristics of the resulting NCs can be controlled. [16,42,43] Colloidal NCs are generally synthesized by reacting precursors (e.g., inorganic salts or organometallic compounds) in solvents in the presence of surfactants. During the reaction, the surfactant molecules not only stabilize the NCs but also tune the reaction kinetics. [44,45] For example, organic ligand molecules are selectively bound to the surface of the growing NCs, which allows the tuning of the growth kinetics of different crystal facets and forms NCs with various shapes, [46–48] such as 1D NCs, [49] tetrapods, [50] nanoribbons, [51] and nanosheets. [52,53]

Thus, as-synthesized colloidal NCs are usually passivated by the organic surfactants having a functional head group (amino-, carboxylic-, thio-, -phosphide) attached on the NC surface and one or several long hydrocarbon chains (C_n , n=8–18). These long-chain ligands, which are used in the synthetic step, give NCs their excellent chemical stability and help in the formation of stable NC colloidal solution in nonpolar organic solvents (e.g., hexane, cyclohexane, chlorobenzene, toluene, etc.). Because the deposition process using NC building blocks is often based on the solution process, the formation of stable col-



Jiwoong Yang received his B.S. (2011) from the School of Chemical and Biological Engineering at Seoul National University. Under the supervision of Prof. Taeghwan Hyeon, he is now working on the synthesis and applications of semiconductor nanocrystals.



Dae-Hyeong Kim received his B.S. (2000) and M.S. (2002) degrees from the School of Chemical Engineering at Seoul National University. He obtained his Ph.D. (2009) from the department of Materials Science and Engineering at the University of Illinois at Urbana-Champaign. Since joining the faculty of the School of

Chemical and Biological Engineering at Seoul National University in 2011, he has focused on stretchable electronics for biomedical and energy applications.



Taeghwan Hyeon received his B.S. (1987) and M.S. (1989) degrees from the Department of Chemistry at Seoul National University. He obtained his Ph.D. (1996) from the Department of Chemistry at the University of Illinois at Urbana-Champaign. Since joining the faculty of the School of Chemical and Biological Engineering

at Seoul National University in September 1997, he has focused on the synthesis and applications of uniform-sized nanocrystals and nanoporous materials.

loids is one of the important prerequisites for NC solutions to be used as "inks". However, in electronic devices, organic ligands are actually insulating barriers for charge transport. Thus, the surface of NCs should be properly treated to obtain well-defined solids and high device performances. One representative way is using ligand exchange with smaller organic molecules (C_n , n = 2-8). It decreases the interparticle spacing in NC solids, which finally improves charge transport.^[54] Short-chain amines,^[55] thiols,^[56,57] pyridine,^[58,59] or hydrazine^[60,61] are commonly used. One drawback of ligand exchange using shorter ligands is that



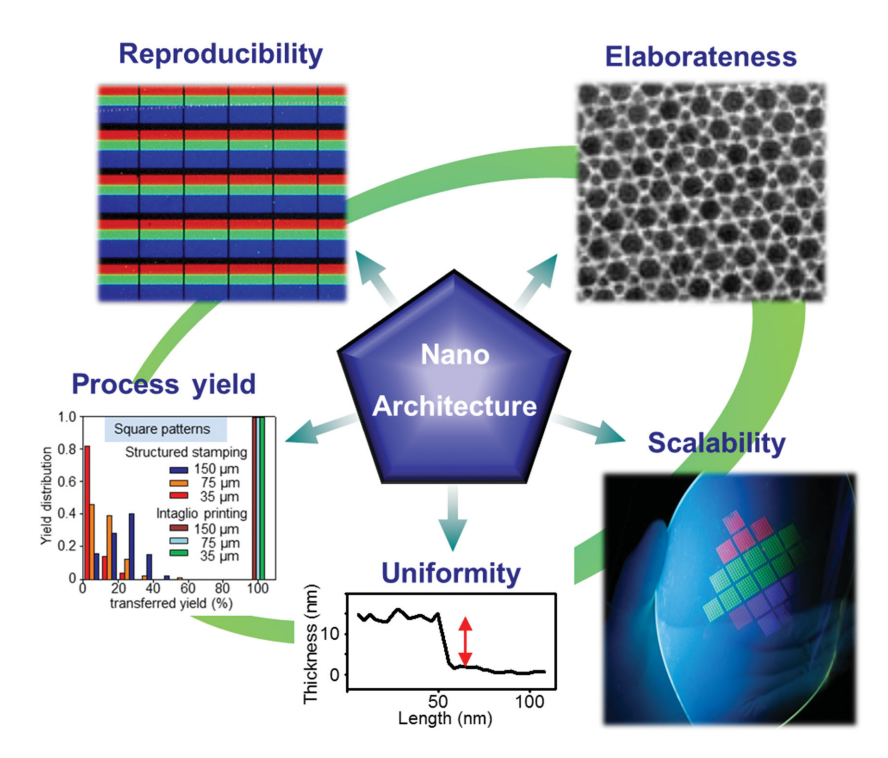


Figure 1. Schematic illustrations describing the important aspects for nanoarchitecture technologies for devices made of colloidal NCs as building blocks. The development of the novel integration/printing process with high reproducibility, elaborateness, scalability, uniformity, and process yield is highly required. Image for "Elaborateness": reproduced with permission. [40] Copyright 2006, Nature Publishing Group. Images for "Reproducibility", "Process yield", and "Scalability": reproduced with permission. [41] Copyright 2015, Nature Publishing Group.

the treatments sometimes decrease the colloidal stability, which possibly results in aggregation of the NCs during/before the deposition process. To prevent this issue, the ligand exchange can be conducted on the NC solids instead of in NC solutions. In addition, this approach has been successfully adopted for the crosslinking of NCs using organic molecules with two functional groups (e.g., diamines, [62] dithiols, [63] etc.). Crosslinking of NCs enhances the electronic transport by increasing the electronic coupling between neighboring NCs as well as reducing the interparticle distance. Although the above approaches dramatically increase the conductivity in NC solids, the use of organic molecules has intrinsic limitations in device applications. For example, many of these small molecules are easily

degradable and volatile, which hampers stable device operation in long-term use. This facilitates the development of inorganic ligands. Since Talapin's group suggested metal chalcogenide complexes (e.g., SnS₄²⁻, In₂Se₄²⁻) as efficient capping ligands for colloidal NCs.^[64,65] tremendous progress has been made, utilizing inorganic ligands in the surface design of NCs. In addition to metal chalcogenide complexes, various inorganic compounds, including metal-free chalcogenides, [65,66] oxometallates, [67] and halide/halametallates,^[68] have been studied for all-inorganic NC solids.[69]

2.2. Casting

One of the simplest film-formation methods is the casting of the colloidal NC solution on a target substrate. Casting readily generates closely packed NC films. The order of the NC film depends on the kinetics of the deposition process. The surface of the substrate is often modified by a self-assembled monolayer of organic molecules to assist the formation of highly uniform films.^[60,70] Two representative methods for casting, drop casting and spin coating, have been widely used and are presented in this section.

Drop casting proceeds by casting drops of the NC solution on a target substrate, fol-

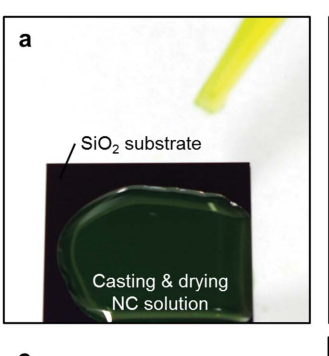
lowed by the simple drying of the cast film (Figure 2a). This is the simplest method, requiring no expensive equipment. For example, NCs having long-chain hydrophobic surface ligands, such as trioctylphosphine or oleic-acid-capped CdSe, InP, or PbSe NCs in hexane or octane, form uniform films through this method. [60,71,72] Sometimes, a superlattice of self-assembled NCs can be made. However, it is generally difficult to control the uniformity and thickness of the overall films by this method (Figure 2b), since the final morphology is mainly determined by the drying step. The evaporation of the solvent at the liquid/vapor interface often results in non-uniform films. In particular, the edge thickness is usually greater than that at the center. This non-uniformity is the major factor that decreases

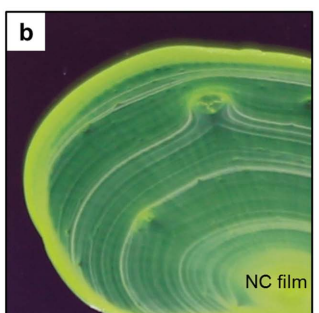
Table 1. Comparison of the film-forming techniques for colloidal NCs.

Туре	Equipment	Waste	Film thickness	Uniformity	Roll-to-roll continuous process
Drop casting	None	Little	Monolayer to several micrometers	Very low	No
Spin casting	Spin-coater	Significant	Monolayer to hundreds of nanometers	High	No
Dip coating	Dip-coater	Little	Monolayer	Moderate	Yes
Langmuir–Blodgett deposition	Langmuir-Blodgett trough	Little	Monolayer to several layers	Extremely high within monolayer	Yes
Doctor blading	Blade	None	Several micrometers	Moderate	Yes

ADVANCED MATERIALS

www.advmat.de





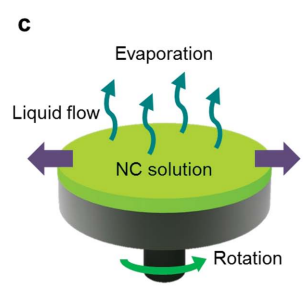




Figure 2. The casting process. a) A photograph showing the drop-casting process. The solution containing CdSe/ZnS QDs was simply cast on the substrate followed by drying. b) A photograph of the NCs film obtained via the drop casting of CdSe/ZnS QDs. Simple casting easily results in inhomogeneous films due to uneven drying. c) Schematic illustration of the spin-coating process. The NC solution is applied onto the substrate during (or before) rotation. d) A photograph showing a spin-coater, which is typically used to control the rotation speed.

the device performance, which is very sensitive to the thickness of the active materials. However, it is not impossible to obtain well-ordered NC solids under strictly controlled material and processing parameters, such as the tight control of the NCs concentration, surface ligands, the volatility of the solvent, the temperature, and the surface condition of the substrate.

To obtain highly uniform films, the spin-coating method is more widely used^[73-76] due to its high uniformity, reproducibility, and simplicity. The process is carried out by casting the NC solution on a rotating substrate (Figure 2c). A spin-coater is used for the precise control of the process parameters, such as the rotation speed (Figure 2d). Most of the solvent on the rotating substrate is ejected by the angular momentum and/or evaporated by spinning, leading to a thin film of NCs remaining on the substrate. The morphology of the final film is mainly governed by the fast spinning step instead of the slow evaporation step in the drop casting. Therefore, the thickness and roughness of the film are determined by the rotational speed, the volatility and viscosity of the solvent, and the concentration of the NCs in the solution. The film thickness (µm), d, in the spin-coating process is expressed by the empirical relationship in Equation (1):[77]

$$d \propto C_0 (\eta_0 D)^{\beta} \omega^{\alpha} \tag{1}$$

where C_0 is the initial NC concentration in the solution (kg m⁻³), η is the initial solution viscosity (kg m⁻¹ s⁻¹), D is the solute diffusivity (m² s⁻¹), ω is the angular velocity (rad s⁻¹), and ω and β are empirical constants. Further theoretical details on the

spin-coating process are available in the literature. [78] In general, it is known that the constants α and β are not significantly affected by the material systems [79] and η and D increase with C_0 . Therefore, the actual control of film thickness is achieved by changing the concentration of the solution and the rotation speed. Practical examples/ranges of conditions used for NC deposition in each application are presented in Chapter 3.

Although spin coating is useful, the process has some limitations. First, more than 90% of the initial solution is wasted during the rotation, and only a small portion of the NCs are used for the film formation. Second, the process cannot produce designed patterns, unless additional lithography procedures are involved. Thus, advanced technologies are required for 2D/3D structured NC solids.

2.3. Dip Coating

Dip coating is a widely used, simple film-formation technique for colloidal NCs (**Figure 3**a,b). [80-83] The substrate is immersed in the NC solution and then retrieved at a controlled rate. An NC thin-film layer is deposited on the substrate as it is removed from the solution. Since the film thickness is mainly determined by the withdrawal speed, the retrieval rate must be well controlled. The coating thickness (m), h, is theoretically expressed by the Landau–Levich equation (Equation (2)):[81]

$$h = c \frac{(\eta U)^{\frac{2}{3}}}{\gamma_{l_{0}}^{\frac{1}{6}}(\rho g)^{\frac{1}{2}}}$$
 (2)

where c is a constant (0.944 for Newtonian liquids), η is the liquid viscosity (kg m⁻¹ s⁻¹), U is the withdrawal speed (m s⁻¹), γ is the liquid–vapor surface tension (kg s⁻²), ρ is the density of the solution (kg m⁻³), and g is the gravitational acceleration (m s⁻²). The operating factor for the process is the withdrawal speed, and the other terms in the Equation (2) can be fixed by regulating the environmental conditions (i.e., temperature, humidity, vapor pressure, etc.) for the given material. Thus, in practice, the thickness of the final film is finely adjusted from a few nanometers to hundreds of nanometers by changing the withdrawal speed. The tendency is well displayed in Figure 3c.

Although dip-coated films are often interrupted by processrelated edge effects (for example, the Marangoni effect^[86] results in zones with irregular transitions at the upper margin during the immersion step, which is caused by variations in the surface tension), the problem can be overcome by scaleup. For example, Murray's group[85] reported the formation of a superlattice on the wafer scale, based on the dip-coating process (Figure 3c-e). In addition, one important benefit of the dip-coating process is that it can be conducted as a continuous roll-to-roll process, which is easily adaptable for the large-scale continuous production. In fact, dip-coating processes are wellestablished in industry, with a history traceable to the 1940s.^[87] Double-sided coating processes are particularly advantageous for the production of optical filters and antireflection coatings for glass products (e.g., displays and lighting). Moreover, the process works well even on nonflat substrates. These



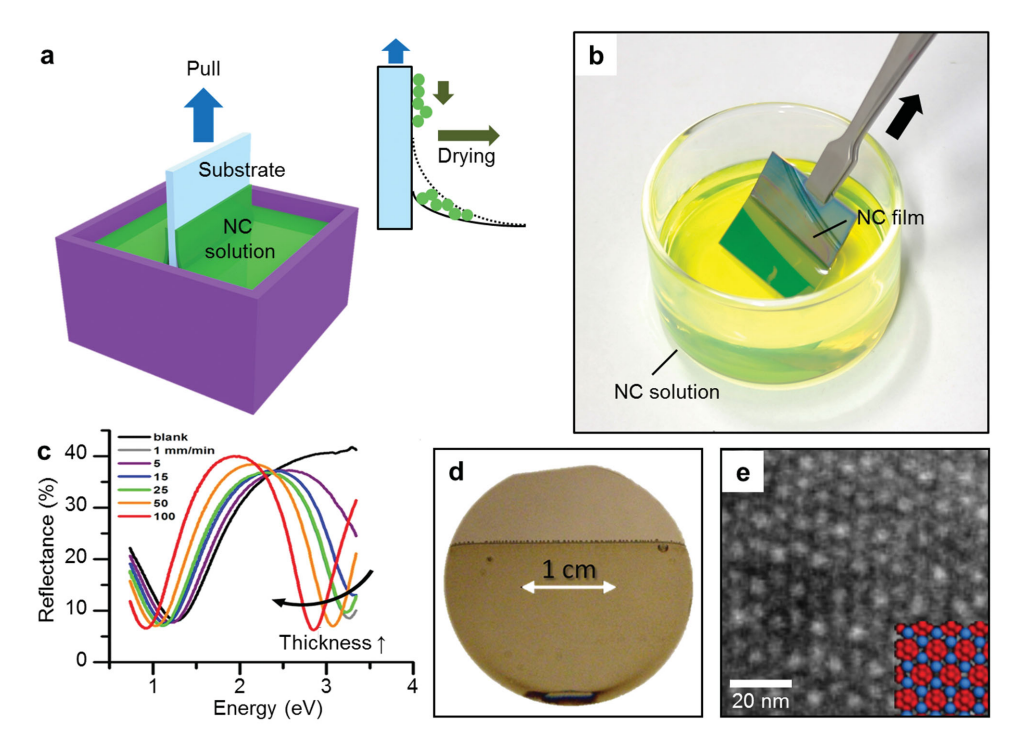


Figure 3. The dip-coating process. a) A schematic of the dip-coating process. b) A photograph showing the dip coating of CdSe/ZnS QDs onto a Si substrate. c) Reflectance spectra of PbSe NC thin films deposited on n-octyltriethoxysilane-treated Si wafers with 250 nm of the thermal oxide by the dip-coating process. The data were measured at various withdrawal speeds: 1 (gray), 5 (violet), 15 (blue), 25 (green), 50 (orange), and 100 (red) mm min⁻¹. For comparison, the reflectance spectrum of an uncoated substrate is also shown (black line). The thicknesses of the final films become larger as the withdrawal speed increases. d) A photograph of a thermally oxidized Si wafer (diameter = 25 mm) dipped into a co-dispersion of PbSe and PbS NCs at a withdrawal rate of 25 mm min⁻¹. e) An SEM image of a polycrystalline binary superlattice in the MgZn₂ phase assembled from PbSe and PbS NCs. The scale bar is 20 nm. c–e) Reproduced with permission. [85]

advantages enlist this approach as a strong candidate that is suitable for NC-based coating processes for industrial areas.

2.4. Langmuir-Blodgett Deposition

Langmuir–Blodgett (LB) deposition, which was initially devised for amphiphilic organic molecules, [88] is a powerful method for obtaining self-assembled monolayers of NCs. NC films can be fabricated by the successive deposition of individual NC LB layers on a target substrate. The presence of organic ligands at the surface of the colloidal NCs makes them appropriate for the LB process.[89–96]

The LB deposition process (**Figure 4**a) for NCs is similar to that used for organic materials. First, the NC layer is formed by spreading the NCs on a liquid surface. The surface pressure, which can be adjusted by moving one or two sliding barriers on the liquid surface, is one of the most important parameters in controlling the morphology of the final film. Figure 4b shows a typical surface-pressure—area isotherm (π –A) for 0D NCs.^[97] The NCs are very loosely packed initially (region I). At a certain point, the surface pressure starts to rise more rapidly, indicating a phase transition and the formation of a complete monolayer (region II, A_1). Further compression results in a small pressure increase (the plateau in region III). This indicates the collapse of the monolayer and formation of a double layer (region IV, $A_1/2$). A similar isotherm and phase transition are observed

again for the formation of the triple layer (region V, $A_1/3$). After the formation of the NC layers with the desired packing density and thickness, they can be transferred to a target substrate through a vertical dipping–pulling process. Sometimes, the NC layer is transferred through a horizontal contacting/lifting process, known as the Langmuir–Schaefer technique.

To obtain a uniform NC layer and control the packing density (or coverage), the surface pressure is precisely controlled by installments (e.g., the LB trough in Figure 4c). Many groups have successfully applied this technique to generate NC films of various materials and shapes, such as nanodots, $^{[89-92]}$ nanocubes, $^{[93]}$ nanorods, $^{[94]}$ and NWs (Figure 4d,e). $^{[95,96]}$ Further delicate control can be achieved by incorporating charged molecules, such as DNA. $^{[99]}$ Sometimes, NCs can be synthesized in situ on ligand films deposited by the LB process. Precursors are selectively attached to a surfactant layer at the air/water interface, and converted into NCs upon the subsequent exposure to reaction gases. For example, some groups have reported the synthesis of metal-sulfide NCs by the reaction between cation precursors and $\rm H_2S$ gas. $^{[100]}$

There are several limitations of the LB technique. The NCs and substrates need to be typically exposed to water, because the assembly process is usually conducted at the water/air interface. This can cause serious problems, particularly in moisture-sensitive materials. Many materials (e.g., conductive polymers and organic molecules) employed in NC-based devices, as well as NCs themselves, are easily damaged by water. Another





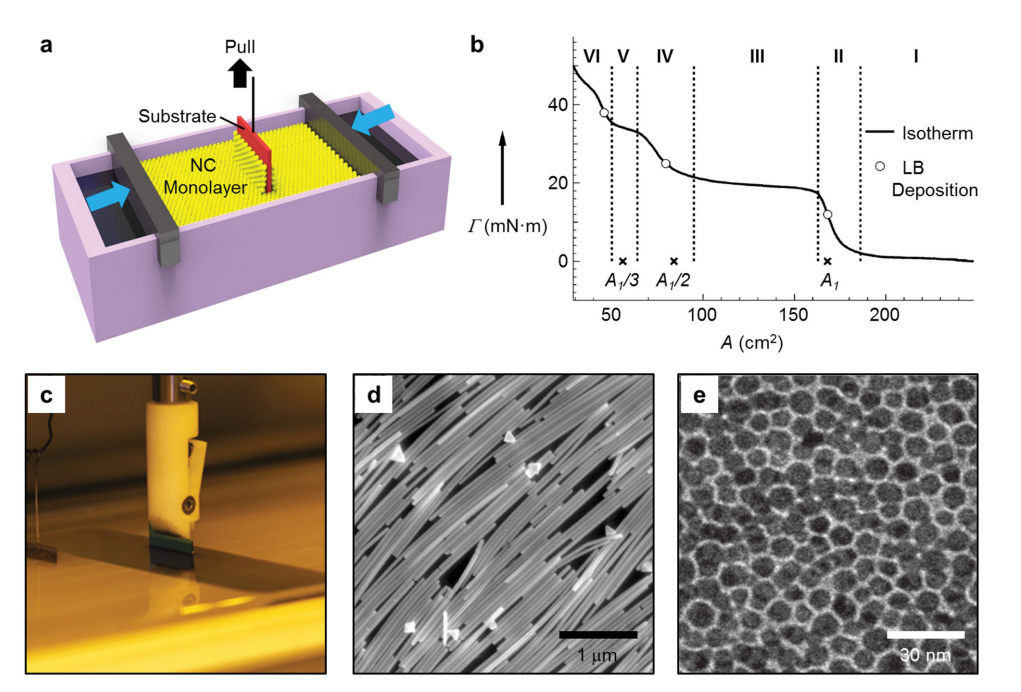


Figure 4. The Langmuir–Blodgett (LB) deposition. a) A schematic showing the LB deposition process. An LB monolayer of NCs is coated on the substrate at the water/air interface. b) A typical pressure–area isotherm of CdSe QDs spread on a water surface. Various regions (I, II, III, etc.) show different phase stages. A₁ represents the area in which the initial full monolayer forms. c) A photograph showing the LB trough. d) An SEM image of monolayer silver NWs acquired by LB deposition. e) A TEM image of monolayer gold NPs acquired by the LB deposition. b) Reproduced with permission. [95] d) Reproduced with permission. [95] Copyright 2003, American Chemical Society. e) Reproduced with permission. [98] Copyright 2014, Nature Publishing Group.

limitation is the difficulty of the large-scale production due to narrow and sensitive processing conditions associated with ultrathin LB films floating on liquids. Further details on LB techniques for colloidal NCs can be found elsewhere. [101,102]

2.5. Doctor Blading

Doctor blading is a representative film-fabrication method for NC films in a relatively thick thickness range (**Figure 5**a). A sharp plate (or a blade) moves over the NC solution on a substrate, which leaves an NC film of uniform thickness. The final thickness of the NC film is determined by the gap between the blade and the substrate. The shape of the meniscus between the blade and the coating solution affects the morphology of the film. The final thickness of the film (μ m), d, is expressed by Equation (3):^[103]

$$d = \frac{1}{2} \left(g \frac{c}{\rho} \right) \tag{3}$$

where g is the gap between the blade and the substrate (μ m), c is the concentration of NCs in the solution (kg m⁻³), and ρ is the density of the material (kg m⁻³). Thus, the thickness of the film is mainly determined by the gap between the blade and the substrate, as well as the concentration of the NC solution.

As shown in Figure 5b, doctor blading produces relatively thick NC films (up to several micrometers). [104] For example, the process has been employed to obtain several-micrometer-thick TiO₂ NC layers in dye- or QD-sensitized solar cells, [106–108] or electrodes made by conducting NCs (Figure 5c). [105] As an advanced/modified method of doctor blading, Mayer rods, periodical grooved rods, or wire-wound rods, have been employed in the blading procedure to make a uniform film

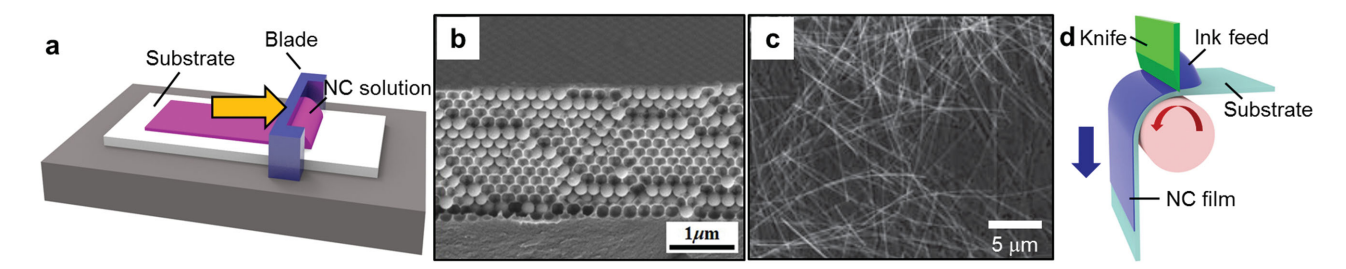


Figure 5. The doctor-blading method. a) A schematic illustrating the doctor-blading process. b) A photograph showing a SiO_2 NC layer coated on a Si wafer by the doctor-blading method. c) An SEM image of a Ag NW network on brass. d) A schematic illustration showing the knife-over-edge process, which is a modified version of doctor blading that is compatible with the roll-to-roll process. b) Reproduced with permission.^[104] Copyright 2014, American Institute of Physics. c) Reproduced with permission.^[105]

thickness without a spacer. In this process, the groove or the wire acts as a spacer of the blading procedure and determines the coating thickness.

Another benefit of doctor blading is its compatibility with roll-to-roll processes. One example is the knife-over-edge coating method, which is similar to normal doctor blading, except for the fact that the position of the blade is fixed while the substrate moves (Figure 5d). One limitation of doctor blading is that it cannot produce an ultrathin NC film with only a few NC layers (i.e., ultrathin thickness), since the thickness of the NC film is determined by the physical gap between the blade and the substrate, which is hard to control on the nanometer scale. Furthermore, there is the possibility of aggregation or crystallization of NCs during the process, since slow evaporation of the solvent takes place after the blading.

2.6. Nanocrystal Superlattices

In this section, we briefly discuss a special case of NC solids, the so-called NC superlattice, in which highly uniform NCs (with standard deviation in particle size less than 10%) selfassemble to form long-range-ordered structures. Because the position of the NCs is precisely controlled and uniform throughout the NC solid, this arrangement can be ideal for device applications as well as fundamental kinetic and thermodynamic studies.

NC superlattices are usually generated upon the slow evaporation of solvent or the gentle destabilization of the NC solution. Various film-fabrication methods, including casting, dip coating, and LB deposition, can be used. Some representative examples of self-assembled NC superlattices are shown in Figure 6. Monodisperse spherical NCs usually form face-centered cubic (fcc) lattices.[71] The ordering of the NCs is explained by thermodynamic principles. Theoretical calculations show that the entropy of the spherical particles can be minimized by forming the fcc phase, [109,110] which is consistent with many previous reports (Figure 6a). Since the free-energy differences between fcc and other packing symmetries are not very large, the modification of the shape anisotropy or dipolar interactions can result in other packing symmetries, such as hexagonal close packing (hcp).[111] Figure 6b shows an example of the hcp superlattice of self-assembled CdSe NCs. Figure 6c compares the fcc and hcp packing symmetries. The self-assembly of 1D nanorods with high shape anisotropy occasionally leads to the formation of liquid-crystalline (nematic and smectic: Figure 6d) and crystalline phases (Figure 6e).[112,113]

A superlattice can be composed of two different kinds of colloidal NCs. These are called binary NP superlattices (BNSLs),[40,114-116] and representative examples are shown in Figure 7a-d. Combinations of metal, metal-oxide, and semiconductor NCs result in the formation of superlattices with particle stoichiometry of AB, AB₂, AB₃, AB₄, AB₅, AB₆, and AB₁₃, with cubic, hexagonal, tetragonal, and orthorhombic symmetries. The most commonly observed phases are shown in Figure 7e. The ratio of the NC radii (R_B/R_A) and the relative amount of each NC species (i.e., particle stoichiometry) determine the final structure of the superlattice (Figure 7f). Compared to superlattices comprising single monodisperse NCs, BNSLs have the greater structural diversity. Therefore, it is challenging to understand their mechanisms of formation. By combining two colloidal NCs with different sizes or electronic/magnetic characteristics, additional degrees of controllability and complexity can be achieved.

The lateral size of the long-range-ordered domain in a superlattice is usually on the micrometer scale. Although recent work^[85] from Murray's group has demonstrated the wafer-scale production of NC superlattices, such a large-area production

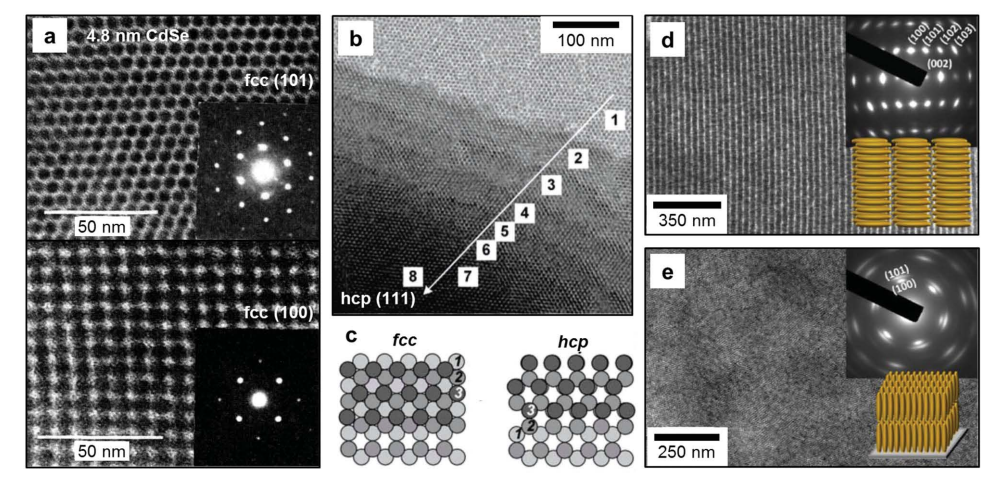


Figure 6. Nanoparticle superlattices. a) Transmission electron microscopy images of the face-centered-cubic (fcc)-packed superlattice self-assembled from 4.8 nm CdSe NCs. Images in the <100>_{SL} and <101>_{SL} projections are displayed. The insets are small-angle electron diffraction patterns showing the ordering in each orientation. b) A TEM image of the hexagonal close packed (hcp) superlattice self-assembled from 5.8 nm CdSe NCs. The image is in the <1111>_{SL} projection. The numbers labeling the NC layers show the ABAB... stacking, which is characteristic of hcp lattices. c) Illustrations showing the differences between the fcc and hcp packing structures. d) Horizontally aligned superlattice of CdSe/CdS 1D dot-in-rod NCs formed on ethylene glycol. e) Vertically aligned superlattice of CdSe/CdS dot-in-rod NCs formed on ethylene glycol. The schematic cartoons indicate the structures of the superlattices. a) Reproduced with permission.[71] Copyright 1995, American Association for the Advancement of Science. b,c) Reproduced with permission.[111] Copyright 2007, American Chemical Society. d,e) Reproduced with permission.[113] Copyright 2015, American Chemical Society.

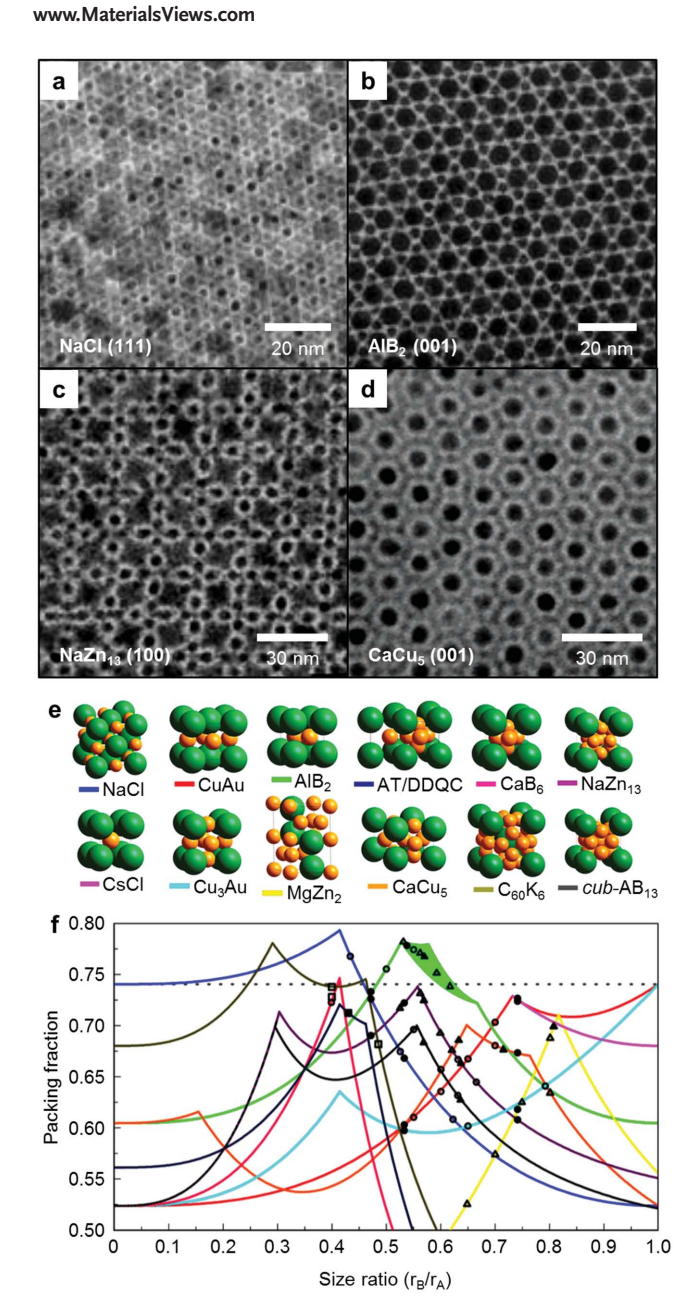


Figure 7. Binary NP superlattices (BNSLs) self-assembled from various semiconductor, metal, and metal oxide NCs. Transmission electron microscopy images of the superlattice assembled from: a) 13.4 nm γ -Fe₂O₃ and 5.0 nm Au NPs, forming a NaCl phase; b) 6.7 nm PbS and 3.0 nm Pd NPs forming an AlB₂ phase; c) 7.2 nm PbSe and 4.2 nm Ag NPs forming a NaZn₁₃ phase; and d) 8.1 nm CdTe and 4.4 nm CdSe NPs forming an AB₅ phase. e) Unit cells of structural models for 12 commonly observed binary NP superlattices. f) Plot of packing density of the models shown in (e) according to the sphere radius ratio ($R_{\rm B}/R_{\rm A}$). The dotted line represents close-packed monodisperse hard spheres. a–c) Reproduced with permission.^[114] Copyright 2006, Nature Publishing Group. d) Reproduced with permission.^[114] Copyright 2007, American Chemical Society. e,f) Reproduced with permission.^[116] Copyright 2007, American Chemical Society.

is not easily achievable. Various interacting forces, such as van der Waals, Coulombic, dipole, entropic, capillary, convective, and shear forces, are involved, [117-120] which add additional complexity to the process and system. Furthermore, these

forces are relevant to characteristics of both the inorganic NC cores and organic surface ligands.^[121] Thus, delicate control of these NC superlattices throughout the entire periodic structure is significantly challenging. These limitations have so far hindered practical device applications.

3. Pattern Printing Methods

For the fabrication of high-density integrated electronics and optoelectronics, the colloidal NC films/solids must be patterned with a high spatial resolution. Advances in patterning technologies have enabled the generation of complicated NC patterns on various substrates, including flexible and stretchable ones, as well as 3D surfaces. In this chapter, we discuss the various patterning methods for NCs. The key characteristics of the various methods are summarized in **Table 2**.

3.1. Screen Printing

Screen printing is a very simple, but fast and efficient patterning technique that has been successfully applied to colloidal NCs (**Figure 8**a). It can produce a large number of nearly identical patterns in a single printing step under ambient conditions and at low cost. In some aspects, the process is similar to doctor blading, except that a patterned screen is introduced. The ink penetrates the open windows/patterns of the screen and is laminated on the target substrate. To prevent any leakages crossing the designed pattern, the ink for the screen printing must have a certain viscosity. Polymers such as poly(methyl methacrylate) are often used as binders with the NCs in the ink to better adhere them to each other and to the substrate. $^{[122]}$ For screen printing, the film thickness (μ m), d, is expressed by Equation (4):

$$d = k_{\rm d} \left(\frac{V}{A}\right) \left(\frac{c}{\rho}\right) \tag{4}$$

where $k_{\rm d}$ is the deposition yield, V is the volume of the solution (mL), A is the open area of the screen (m²), c is the concentration of the NCs in the solution (kg m³), and ρ is the density of the material in the NC film (kg m³). The deposition yield ($k_{\rm d}$) is affected by many factors, including the snap-off distance, the speed of the blade, the viscosity of the solution, and the force against the screen. The yield should be maintained for a repeated process to get homogeneous film reproducibly.

The advantages and limitations of screen printing are similar to those of doctor blading. Screen printing is economical and compatible with roll-to-roll processes. For example, roll-to-roll rotary screen printing has been developed. Due to the requirement of a relatively high viscosity of the inks, the films are generally thick (greater than hundreds of nanometers). Thus, the technique is suitable for making interconnections or electrodes based on conducting metal NCs^[123,124] (Figure 8b) and thick TiO₂ NC layers^[125] in electronic circuits and dye-sensitized solar cells, respectively. Sometimes, binders, usually organic materials, cause the increase of resistance and should be treated

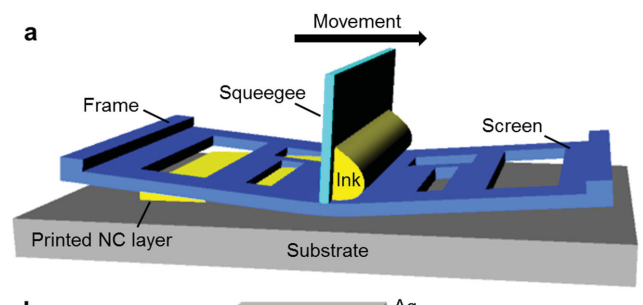
Table 2. Comparison of the printing techniques for colloidal NCs.

Туре	Equipment	Pattern width	Film thickness	Roll-to-roll continuous process
Screen printing	Screen printer	millimeters	Several micrometers	No
Inkjet printing	Inkjet printer	ca. micrometers	Several micrometers	No
Nanoimprinting	Mold or stamp	tens of nanometers	Several micrometers	Yes
Microcontact printing	Stamp	ca. 60 nm	monolayer	Yes
3D printing	3D printer	micrometers	N.A.	Yes

properly. The resolution of the final pattern is determined by that of the screen.

3.2. Inkjet Printing

Inkjet printing is an attractive technique for the microscale patterning of various materials. [126-129] A schematic inkjet-printing procedure is shown in **Figure 9a**. The ink (homogeneously dispersed NCs in a solvent) is ejected as tiny droplets (with micrometer-scale diameters) by an applied electric field and pressure, and is directly deposited at the desired substrate locations. This is the most-economical printing method among the various NC patterning processes due to its minimal mate-



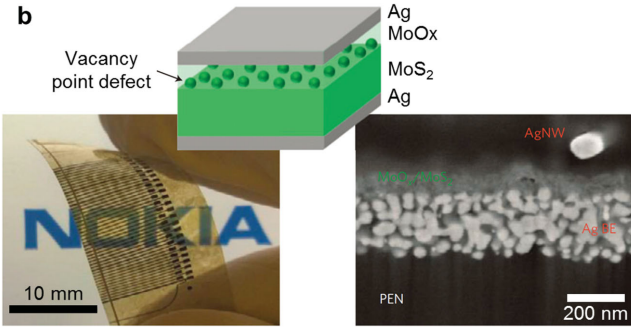


Figure 8. The screen-printing process. a) A schematic illustrating the screen-printing process. The screen is used to obtain patterns. b) Solution-processed MoO_x/MoS_2 memristors on a plastic foil. The bottom and top electrodes were fabricated, respectively, by inkjet printing and screen printing of silver NP ink on a poly(ethylene naphthalate) (PEN) foil. The MoS_2 film was deposited by a spreading technique. The right picture shows a photograph of a cross-point memristor array on PEN with high visual transparency. The scale bar represents 10 mm. The left image shows the cross-sectional scanning electron microscopy image of the Ag NWs/ MoO_x/MoS_2 switching device. Scale bar: 100 nm. The inset cartoon shows a schematic of the vertically stacked Ag/ $MoO_x/MoS_2/Ag$ memristor. b) Reproduced with permission. [123] Copyright 2015, Nature Publishing Group.

rial loss. Because inkjet printing is a non-contact technique, NC inks can be deposited on diverse substrates such as polymers, metals, oxides, and biomaterials. Additional benefits of the inkjet printing are that patterns can be easily changed and that printing over large areas is relatively easy.^[130]

The use of colloidal NCs as dispersions overcomes the solubility limitations of the inks, leading to more-stable printing, [132] However, dispersion-based inks have short shelf-lives due to their easy precipitation or aggregation. Moreover, if the ink volatility and viscosity are not precisely controlled, "coffee-fringe" or central "mountaintop" effects tend to form nonflat films due to capillary [133] or Marangoni [134] flows during the drying of the inks. [135] Coffee-fringe edges often appear when NCs accumulate at the rim of the drying droplet due to the inhomogeneous evaporation of the solvent (Figure 9b). [136] This uneven morphology leads to electrical defects.

To overcome these issues, the evaporation rate has been controlled by introducing additives having a high boiling point and low surface tension. [137,138] Mixed solvents (original solvent and additive agent) afford a surface-tension gradient during drying (Marangoni flow). The main solvent, having a lower boiling point and a higher surface tension, preferentially evaporates at the contact line, resulting in an outward flow. On the other hand, the Marangoni flow developed by the solvent gradient retards the outward flow. These cause the formation of a surface-tension gradient over the whole droplet during drying, which develops an inward flow. The outward and inward flows consecutively circulate the NCs suspended in the ink and lead to a uniform thickness film. [139] Figure 9c presents the uniform surface profile of Al₂O₃ NCs resulting from the use of a co-solvent ink. [131]

Figure 9d shows a typical inkjet-printer system. Generally, the resolution of patterns using NC inks is tens of micrometers and depends mainly on the droplet size, which is affected by the jetting conditions, such as the nozzle diameter, ink viscosity, applied bias, surface tension, and ink density. The Ohnesorge (Oh) number for the printing process is suggested as Equation (5):

$$Oh = \frac{\sqrt{Web}}{Rey} = \frac{\eta}{\sqrt{\sigma \rho d}}$$
 (5)

where "Web" and "Rey" are the Weber and Reynolds numbers for the ink, and η , σ , ρ , and d are the viscosity (kg m⁻¹ s⁻¹), surface tension (kg s⁻²), ink density (kg m⁻³), and orifice diameter (m), respectively. Figure 9e shows the dimensionless widths of inks printed at various droplet pitches compared to the theoretically predicted values obtained from the equation. Although





Droplets
Patterned layer
Substrate

Droplets
Patterned layer



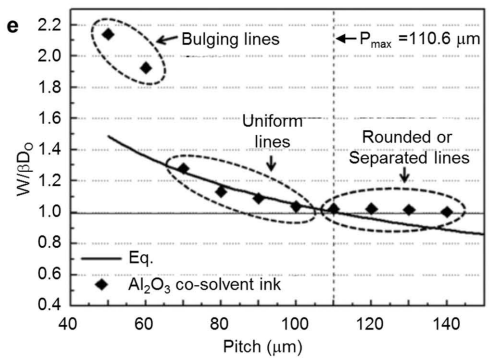


Figure 9. The inkjet-printing process. a) A schematic depicting the inkjet-printing process. A NP solution is ejected as droplets and then deposited on the substrate. The pattern can be obtained by simply changing the input signals. b,c) Scanning electron microscopy images and thickness profiles of Al_2O_3 NP ink patterns. A water single-solvent ink results in a pattern of inhomogeneous thickness (b), whereas a DMF/water co-solvent ink results in a pattern of uniform thickness (c). d) A photograph of the inkjet printer. e) The dimensionless widths of Al_2O_3 NP lines printed at different ink-droplet pitches, compared with the theoretically predicted values (black solid line). b,c,e) Reproduced with permission. [131] Copyright 2011, Elsevier.

the effects of single parameters, such as the concentration, solvent system, blend ratio, and temperature, on the printing have been investigated, the impact of these factors in combination remains unknown.

The inkjet-printing process is easily applied to the fabrication of various kinds of devices, such as LEDs, solar cells, and field-effect transistors (FETs), as well as in the formation of interconnections in electronic circuits.^[140] Figure 10a,b show photoluminescence (PL) images of line^[141] and areal patterns of QDs. These QD patterns can be utilized to fabricate QLEDs. One advantage of this technique is the capability of multiple printing, which can be exploited to print multicolor LEDs in 3D configurations. For example, Figure 10c shows a representative 3D pattern produced by stacking multiple ink patterns. [142] The height of each patterned structure is proportional to the number of stacked layers. Stretchable electrodes can be patterned by printing a mixture of elastomer and conducting NCs.[143] Vertically wrinkled, inkjet-printed, stretchable interconnections are shown in Figure 10d. Inkjet printing allows the formation of stacks of elastomeric inks in a single step without any complex patterning procedures. The substrates are not limited to flat surfaces. By controlling the ink density and solvent volatility, omnidirectional printing can be introduced to realize 3D electrical structures.^[144] Figure 10e presents antenna patterns that were inkjet-printed onto the spherical surface of a glass bowl. Metallic Ag NC inks were conformally laminated onto the curvilinear surface to create the conductive lines of the antenna. Figure 10f presents the scanned pattern of the antenna obtained by optical profilometry, and the inset shows

a scanning electron microscopy (SEM) image. The 20 μm -thick conductive lines with 100 μm widths were successfully formed on the concave structure.

3.3. Nanoimprint Lithography

Nanoimprint lithography (NIL) is one of the most widely used patterning techniques to reach micrometer or sub-micrometer feature sizes (down to tens of nanometer). The merits of NIL are its cost effectiveness, large-scale applicability, simple process, and extremely high resolution below the limit of the light diffraction (comparable with that of e-beam lithography). In NIL, the cast NC layer on the substrate is pressed by a rigid patterned mold/stamp to form NC patterns (Figure 11a). Generally pressing and thermal treatment simultaneously proceed. Polymer-NC composites are typically employed to achieve the uniform film thickness and surface. [146] Tamborra et al. reported luminescent nanocomposites based on CdSe@ZnS NC-PMMA copolymers using micro/nano NIL patterning. These nanocomposites were applied to photonic applications (Figure 11b,c). [147] PMMA, a well-known polymer with good processability, was exploited to assist the NC nanopatterning. Under the conditions of high temperature and pressure, PMMA reflows and fills the gap of the stamp, and thus composite patterns are easily generated with high fidelity.

Solid-state NIL is a powerful tool to achieve fine patterns/ features through a single process. Sometimes, residual raw



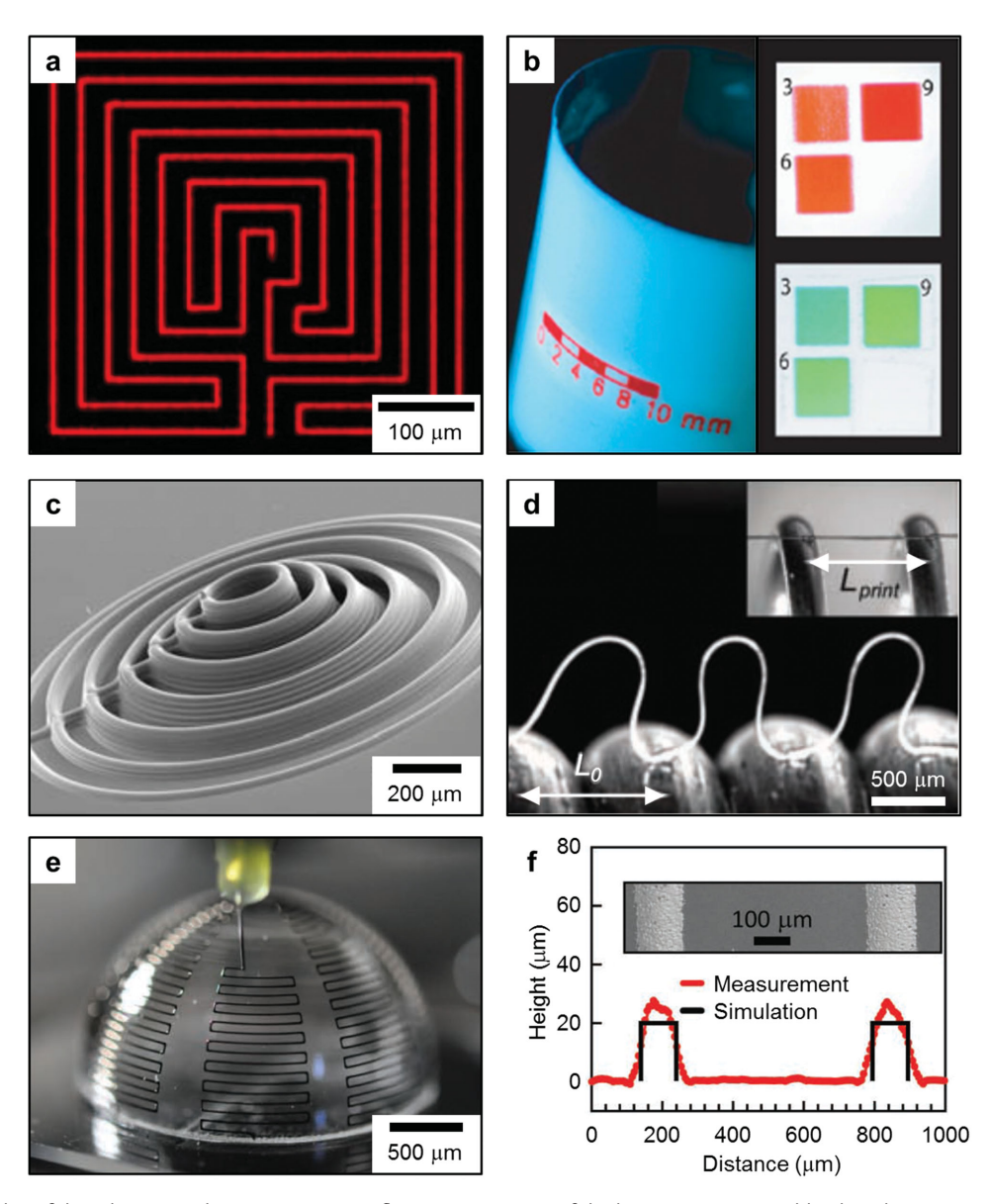


Figure 10. Examples of the inkjet-printed NC patterns. a) A fluorescence image of the line pattern acquired by the inkjet printing of CdSe/CdS/ZnS red QDs in dichlorobenzene. b) A photograph of QLEDs on a flexible substrate under illumination (365 nm). The pattern was inkjet-printed with a red QDs–polyisobutylene composite solution. c) An SEM image of silver microelectrodes patterned with 30 um nozzles using silver NP ink. d) An optical image of stretchable silver arches inkjet-printed onto a spring. e) A photograph of the antenna during printing via a silver meander line. The conformal printing of silver NP inks on the curvilinear surface created conductive meander lines. f) Thickness profiles of the meander lines shown in (e) determined by optical profilometry. The black solid line represents the design simulations of the meander lines. The inset shows the corresponding segments. a) Reproduced with permission.^[140] Copyright 2015, American Chemical Society. b) Reproduced with permission.^[140] c,d) Reproduced with permission.^[140] c,d) Reproduced with permission.^[140] Copyright 2009, American Association for the Advancement of Science. e,f) Reproduced with permission.^[141]

materials remain on top of the patterns after the process. These residues often become defects that degrade the electronic properties of the nanocomposite patterns. Therefore, to remove the residual layer, an elastomeric stamp (e.g., PDMS stamps) is applied to the NC solution (Figure 11d). A drop of NC solution is cast on the target substrate and the stamp presses the droplet on top. The elastomeric stamp is conformally contacted on the target substrate and the NC solution is slowly evaporated. Kagan's group reported a new type of optical metamaterial design using NIL and Au NCs (Figure 11e). [148]

Nanoscale superstructures were fabricated by the NIL process. The dielectric-to-metal transition can be obtained by the post solid-state ligand-exchange process (Figure 11f). In work by Torres's group, [150,149] UV-curable polymers were incorporated with NCs to make nanoscale features. Instead of solvent evaporation, UV solidifies the polymer–NC composites (Figure 11g). The periodically patterned NC layer can be applied to 2D photonic crystals (Figure 11h,i). The light collection of photonic crystal structures is two times higher than that of a flat one.

ADVANCED MATERIALS

www.advmat.de

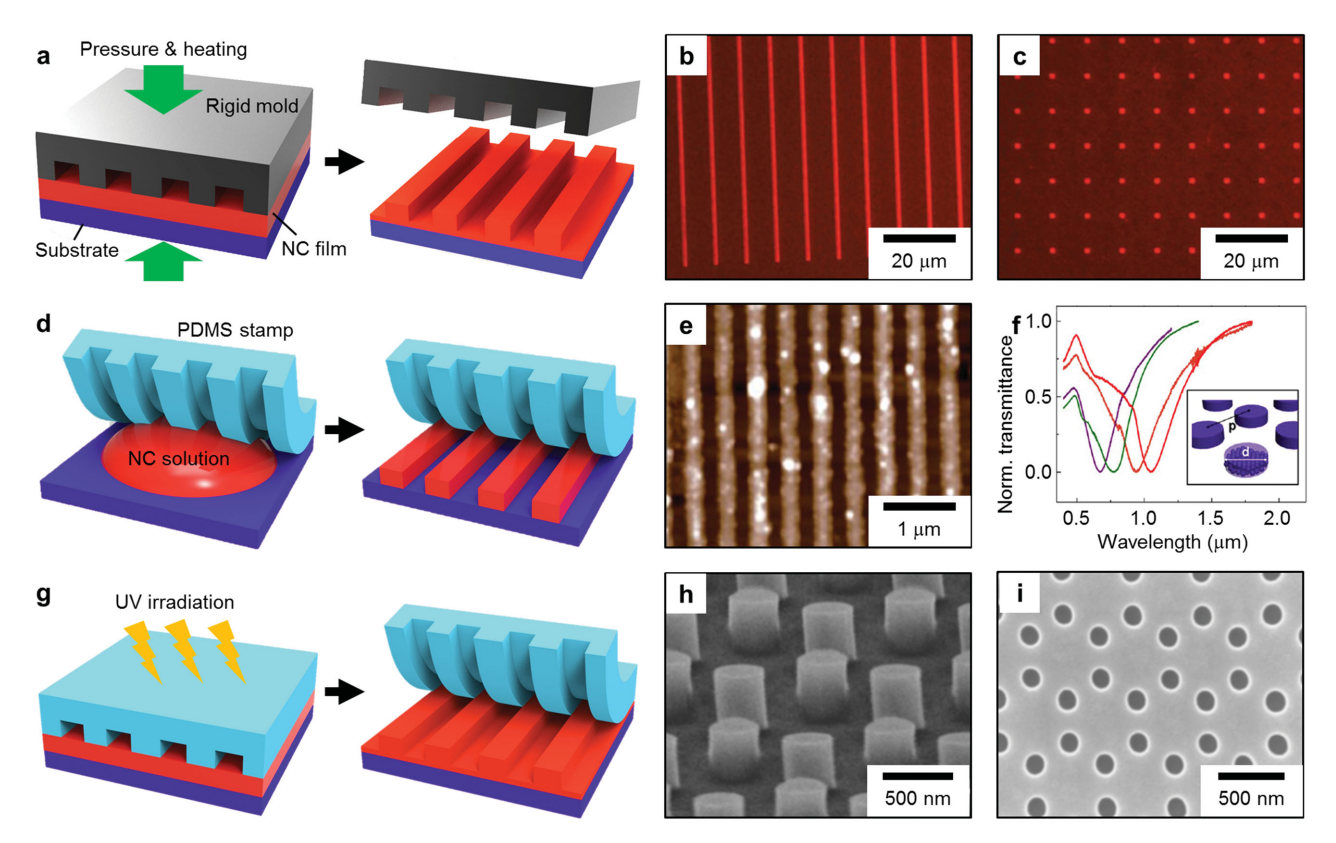


Figure 11. Nanoimprint lithography (NIL). a) A scheme describing solid-state NIL. b,c) PL images of the imprinted CdSe@ZnS NC-PMMA composites in motifs of line and space (b) and dot (c), respectively. d) The illustration of solution-state direct NIL using an elastomeric PDMS stamp. e) Atomic force microscopy (AFM) image of the imprinted SCN-capped Au NC arrays. f) Transmittance spectra of Au-NC-based nanopillars changing in diameter, d and pitch, p. The structural information of periodic nanopillars: red (d = 300 nm, p = 850 nm), orange (d = 270 nm, p = 700 nm), green (d = 200 nm, p = 500 nm), and purple (d = 120 nm, p = 700 nm). g) A scheme describing UV-assisted NIL. The patterns are formed by curing a UV curable resin. h,i) SEM images of the silicon stamp with 2D nanopillars (h) and the nanoimprinted photonic crystals composed of CdSe@ZnS NCs and mr-NIL 6000 resin (i). b,c) Reproduced with permission. (149) Copyright 2013, American Chemical Society. h,i) Reproduced with permission. (149) Copyright 2007, American Institute of Physics.

3.4. Microcontact Printing

Adv. Mater. 2016, 28, 1176-1207

Contact printing is a powerful method for the transfer of NCs in micro-/nanoconfigurations using stamps at desired locations. [151,152] Soft, elastomeric polymers are utilized as stamps to pick up and place the NC "ink" on the target substrate. [153] This room-temperature, low-cost procedure is simple yet powerful, due to the versatile processability of various NCs on different kinds of target substrates. [The contact-printing techniques are categorized into three types: additive transfer, subtractive transfer, and intaglio transfer (Figure 12).

In additive-transfer printing, the NC layer is directly coated on an elastomeric stamp using spin-casting or spray-coating techniques. To transfer this coated "ink" onto the target substrate, a reasonably different work of adhesion between the PDMS/NC interface (W_{12}) and the NC/receiving substrate (W_{23}), yielding $W_{12} > W_{23}$, is needed. The work of adhesion can be calculated by the harmonic mean equation as described in Equation (6):

$$W_{12} = 4 \left(\frac{\gamma_1^d \gamma_2^d}{\gamma_1^d + \gamma_2^d} + \frac{\gamma_1^p \gamma_2^p}{\gamma_1^p + \gamma_2^p} \right)$$
 (6)

where γ is the surface free energy (kg m⁻¹ s⁻²) and the superscripts d and p mean the dispersion and polar components of γ , respectively. If the surface energy of the PDMS stamp (19.8 mJ m⁻²) is substantially lower than that of the target substrate (e.g., >200 mJ m⁻² for glass and silicon), the NC layer is easily transferred from the stamp to the target. In additive-transfer printing, therefore, the quality of the inking process determines the quality of the resulting pattern.

Conventionally, the NC layer is spin-cast on a PDMS stamp. However, due to the possibly poor chemical compatibility between the elastomeric stamp and the organic solvent of the NC solution, the type of solvents is limited, and it is difficult to obtain an evenly coated NC layer. [156] Applying an ultrathin coating on the surface of the PDMS partially solves this problem. Coating layers include parylene, [157] SU-8, [158] and self-assembled monolayers, [159] which change the surface energy, as well as increase the chemical compatibility of the stamps. For example, coating with parylene-C, which contains aromatic groups, decreases the surface energy difference between the QD monolayer and the stamp. [158] Consequently, the contact angle between the PDMS stamp and a QD solution in chloroform decreases from 28° to 6°. This modified surface energy facilitates the wetting of the QD layer on the stamp, as well



b a (1) Contact on QD layer (1) Contact on intaglio trench Structured QD solution QD lave Donor Intaglio substrate trench (1) Spincoating QD layer on the structured stamp (2) Detachment (2) Detachment (3) Transfer (3) Transfer (2) Transfer Target substrate

Figure 12. The microcontact-printing process. a) Schematic showing the additive-transfer-printing method. Colloidal NCs are directly coated on the patterned stamp and then transferred onto the final substrate. b) Schematic showing the subtractive-transfer-printing method. A part of the coated NC film on the donor substrate is selectively detached by the structured stamp. The detached part is transferred onto the final substrate. c) Schematic showing the intaglio-transfer-printing method. A part of the coated NC film on the stamp is selectively detached and removed by the intaglio-patterned trench. The remaining QD film on the stamp is transferred onto the target substrate.

as its release from the stamp. Figure 13a shows an image of two different QD layers cross-transferred using this additive-transfer-printing technique.

Another contact-printing method is subtractive-transfer printing. Figure 13b presents the cross-sectional transmission electron microscopy (TEM) image of the transfer-printed QD monolayer. As shown in Figure 12b, the subtractive-transferprinting process consists of two steps in which the NC layer is picked up from the donor substrate and released from the elastomeric stamp.[161] In contrast to additive transfer, NCs are inked on the stamp by picking up the NC layer from a donor substrate. Therefore, the surface energy of the donor substrate must be similar to or lower than that of the stamp. The surface energy of a silicon wafer as the donor substrate can be lowered by coating it with a self-assembled monolayer of octadecyltrichlorosiloxane (ODTS).[160] The wetting of the QDs on the donor substrate is also promoted by the aliphatic ligands of the ODTS. As the surface energy of the donor substrate is similar to that of the elastomer stamp, dynamic parameters such as the retrieval rate and time-dependent application of pressure must be controlled to maximize the transfer-printing yield. Figure 13c shows the relationship between the pick-up rate and the resulting yield. The separation energy at the QD/ stamp interface, $G_{\text{OD/stamp}}$, depends strongly on the peeling rate, as described in Equation (7):

$$G^{\text{QD/stamp}} = G^{\text{QD/donor substrate}}[1 + \phi(\nu)] \tag{7}$$

where ϕ is a function of the velocity (ν , m s⁻¹) and $G_{\rm QD/donor}$ substrate is the separation energy (kg m s⁻²) at the interface of the QD and donor substrate. As shown in Equation (7), the transfer yield is mainly determined by the pick-up rate. The graph shows that nearly perfect transfer of QDs (over 90%) can be

achieved at the critical peeling rate, for instance, of 60 mm s⁻¹, with an applied pressure of 196 kPa, or 80 mm s⁻¹ at 98 kPa (Figure 13c). The QDs are quickly picked up by the stamp and slowly released on the target substrate. This technique has been used to fabricate red, green, and blue (RGB) pixelated active-matrix QLEDs. Tightly packed, subtractively transferred, and defect-free QD layers lead to QLEDs with electroluminescence (EL) properties that are more efficient than those fabricated by the spin-coating process (Figure 13d). Electroluminescent white LEDs have also been demonstrated by vertically stacking RGB QD layers to minimize energy transfer within the active layer.^[70]

The final transfer-printing method is the intaglio-printing method. Although the subtractive-transfer technique is a powerful tool for transferring NC layers onto target surfaces, the pick-up yields are dramatically decreased as the pattern size decreases.[41] Due to the applied pressure during the transferprinting process, stresses and thereby cracks in the NC layer are induced at the edges of the stamp structure during the rapid pick-up process. Delamination of the NC layer often takes place, which results in the shrinkage of the QD patterns and consequently impedes the fabrication of high-definition RGB pixels. In intaglio-transfer printing, the pick-up process is identical to that in subtractive transfer, but with a flat stamp instead of a patterned one (Figure 12c). The picked-up QD layer on the flat PDMS stamp is laminated on an intaglio-patterned trench. As the interfacial energy of the PDMS/QD is much less than that of the QD/trench, the part of the QD layer in contact with the trench is transferred onto the surface of the trench and the rest of the QDs remain on the PDMS stamp. The residual QD pattern on the PDMS stamp is transferred to the target substrate. As an example of this process, the high-density aligned





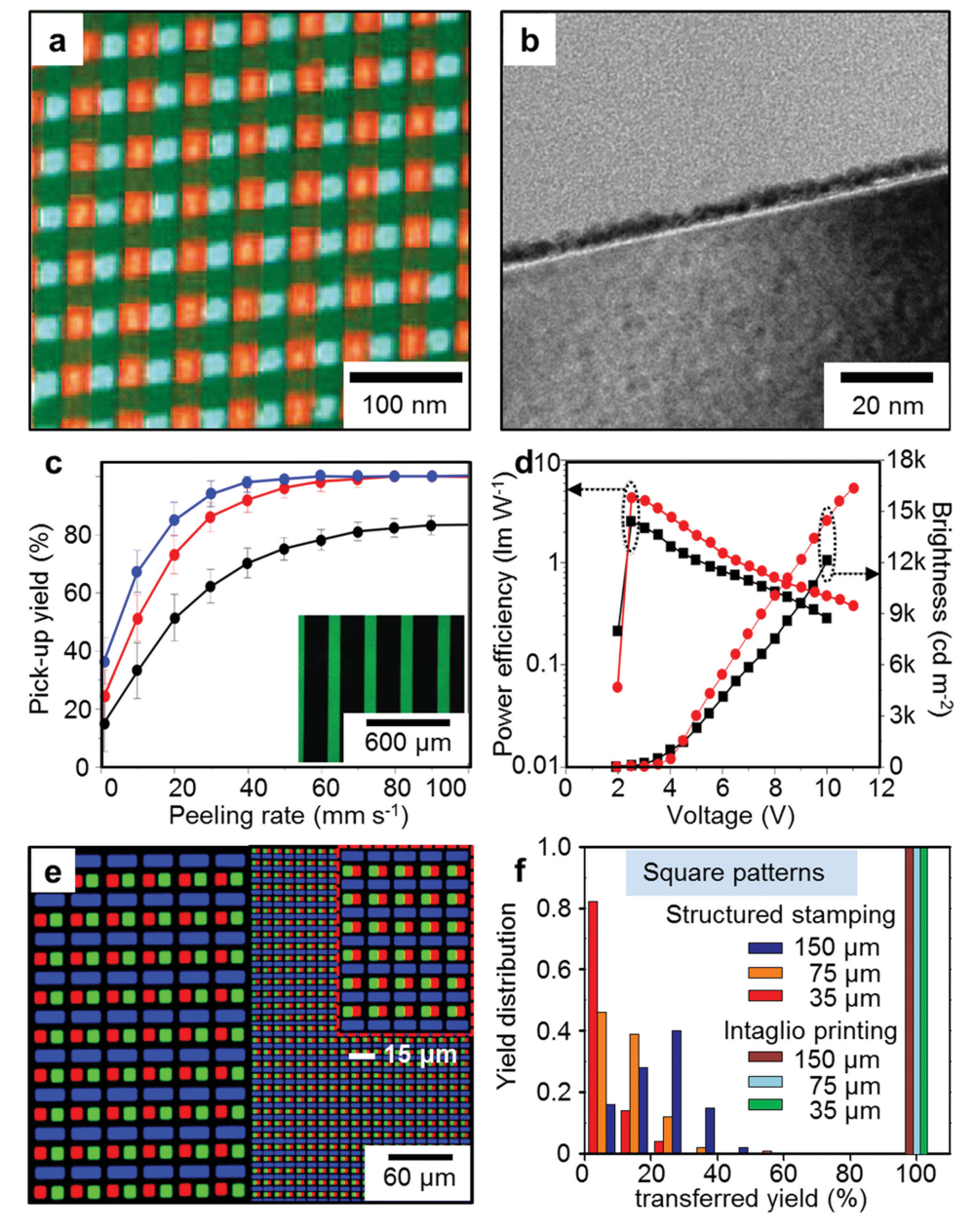


Figure 13. Examples and characteristics of transfer-printed NC patterns. a) Electroluminescence of QLEDs with an emissive layer consisting of 25 µm-wide lines of green and red QD monolayers at an applied bias of 7 V. The line pattern was produced by the subtractive transfer-printing method described in (b). The blue emission is from a TPD (N,N'-bis(3-methylphenyl)-N,N'-diphenylbenzidine) hole-transporting layer. b) A cross-sectional transmission electron microscopy image of a QD monolayer on a Si substrate. The scale bar represents 40 nm. c) Pick-up yield of QD layers according to the peeling velocity during lift-off of the stamp in the subtractive transfer process. The error bars show the standard deviation of the pick-up yields measured at different pressures. d) Comparison of the luminous efficiency and brightness versus voltage characteristics of QLEDs fabricated by the subtractive transfer printing (red circles) and the spin coating (black squares) of red QDs. e) Photoluminescence images showing aligned red-green-blue pixels obtained by the intaglio transfer printing of QDs. The resolutions are 882 pixels per inch (left) and 2460 pixels per inch (right). f) Distribution of printing yields at different pattern sizes (150, 75, and 45 mm) using two different transfer-printing methods (subtractive and intaglio transfer printing). The yields for the subtractive stamping dramatically decrease with pattern size, whereas that of the intaglio printing is maintained near 100%. a) Reproduced with permission.^[157] Copyright 2008, American Chemical Society. b) Reproduced with permission.^[170] Copyright 2014, Nature Publishing Group. c,d) Reproduced with permission. [160] Copyright 2011, Nature Publishing Group. e,f) Reproduced with permission. [41] Copyright 2015, Nature Publishing Group.

transfer of RGB QD patterns up to 2460 pixels per inch is shown in Figure 13e. Regardless of the pattern size, a transfer yield of nearly 100% was achieved with this transfer method (Figure 13f).

3.5. 3D Printing

3D printing is an emerging additive printing technique for 3D objects.[162-164] Unlike traditional subtractive manufacturing



www.MaterialsViews.com

processes, such as cutting or knifing, this additive printing stacks 2D patterns layer-by-layer to from 3D structures. 3D printing has been utilized to mimic natural microstructures (e.g., repeated microstructures of butterfly wings, porous bone structures, etc.) and/or to scale down man-made constructions/ objects (e.g., micrometer-sized miniature cars). As 3D-printing technology advances, brand-new characteristics/shapes that cannot be achieved in nature have been demonstrated. This progress has been accelerated with the rapid development of novel composites and/or multifunctional materials designed for 3D printing. Smart 3D structural design concepts, with the assistance of computers and vigorous application of 3D printing in industry, electronics, and biology further encourage new findings and research results.[165] For instance, computeraided structural designs suggest new types of damage tolerant hierarchical structures having a high tensile strength (1.75 GPa) with deformable characteristics.^[166] As the 3D shaping/stacking process is computer-controlled, the geometric complexity of the target design does not limit the applicability of this method. The ability to directly incorporate diverse nanomaterials in inks and to print them in 3D layouts is attractive. Up to now, 3D printing using colloidal QDs is based on the inkjet-printing technique.[167,168]

One of representative examples of 3D-printed colloidal NCs is shown in Figure 14a. The LiFePO₄ NCs are multi-stacked in 3D using inkjet printing for a microscale Li-ion battery. To stack electrode structures reliably, the composition considering the rheology of the NC ink is precisely controlled. The solvent is composed of DI water, ethylene glycol, and glycerol. This composition enables the gradual evaporation of the NC ink, which improves the bonding of individual layers and enhances the uniformity of the NC ink. The thickness of the printed structures proportionally increases to the number of stacked layers. The areal capacities of the 8-layer stacked 3D LiFePO₄-Li₄Ti₅O₁₂ architecture at various C rates are presented in Figure 14b. The results indicate that the Li-ion battery delivers ca. 1.5 mA h cm⁻² under 1.8 V at a 5C rate.

Figure 14c shows the concept of 3D digital projection printing using photo-polymerizable piezoelectric NC-polymer colloidal dispersions.^[170] The NC-polymer dispersion is printed in 3D based on designed patterns. The polymer liquid is photocured in a few seconds and encapsulates the suspended NCs. Figure 14d presents patterned BaTiO₃ NCs in poly(ethylene glycol) diacrylate (PEGDA). Two layers having different thermal expansion coefficients were printed, which thereby caused the film to roll into a tubular structure after being peeled from the substrate. Another example is given by solution-processed QLEDs on spherical surfaces. Figure 14e shows an exploded view of a QLED on a concave lens-like structure.^[169] Diverse "inks" were printed at the desired location of the curvilinear surface to form QLEDs. The resulting device shows stable current–voltage properties (Figure 14f).

4. Applications

By virtue of the various coating and printing methods highlighted in this review, diverse nanomaterials ranging from metal NWs to QDs have been prepared and used in electronic and optoelectronic devices. Nanomaterials serve diverse roles in these devices: as conducting layers or electrodes, semiconducting channels, electron- or hole-transporting layers, and light-emitting or light-absorbing layers. In this chapter, specific applications of the assembled NCs for various electronic devices are reviewed.

4.1. Electrodes

Colloidal metallic NCs have been widely employed to make transparent electrodes, typically in the form of metal NPs dispersed in the ink. Solution processes using NC solutions have advantages over conventional vacuum-evaporation processes, such as low equipment and processing costs, mild operating conditions, and compatibility with large-area electronics. In many optoelectronic devices such as LEDs, solar cells, and photodetectors, a transparent electrode through which photons can pass without absorption, scattering, and/or reflection is an important component. Thin films of doped metal oxides such as indium tin oxide (ITO), aluminum zinc oxide (AZO), and indium zinc oxide (IZO) have been widely utilized as transparent electrodes, both in industry and academia. However, their high stiffness and brittleness limit their use in flexible and stretchable electronics. Their high cost - which continues to increase due to the use of rare elements, including indium - is another challenge in metal-oxide electrodes. Thermally evaporated ultrathin Au or Ag metal films (<20 nm) have been employed as semitransparent electrodes, but the huge loss in emitted or absorbed photon efficiency due to their low transparency is a serious drawback. The ideal performance requirement is high transparency (at least more than 80% for display panels) and low sheet resistance (<100 Ω sq⁻¹). Therefore, various nanomaterials have been investigated as promising alternatives to preceding conventional electrodes. ITO NCs,[171] Ag NPs, Cu NWs,[172,173] and Ag NWs are good examples. In particular, highly percolated Ag NW networks, which exhibit high transparency (ca. 90%) and low resistance (ca. 10 Ω sq⁻¹), are close to being commercially applied in displays, touch panels, and solar cells.

To prepare transparent conducting films of Ag NWs, various processes have been used, including spin coating, [174] spray printing,[175] blading with a Mayer rod, or transfer printing with stamps.[176,177] The thickness of the NW film is usually limited to less than ca. 100 nm to guarantee sufficient light penetration. One disadvantage of conventional NW networks is the disconnection of junctions between the NWs that occurs under repetitive applied strain. Cui's group reported large-scale transparent electrodes with Au-bridged Ag NWs (Figure 15a).[178] Doctor blading of a Ag NW solution with a Mayer rod generated highquality electrodes that showed stable bending characteristics, which could be scaled up for a continuous roll-to-roll process (Figure 15b). To form robust interwire junctions, the Ag NW film was alloyed with Au through the galvanic replacement reaction of Ag by Au. The Au alloy effectively bridged the Ag NWs at their junctions (Figure 15c).

Hybrid Ag NW structures that form strong NW junctions with various organic/inorganic/carbon materials can further enhance the flexibility, conductivity, and processability of Ag





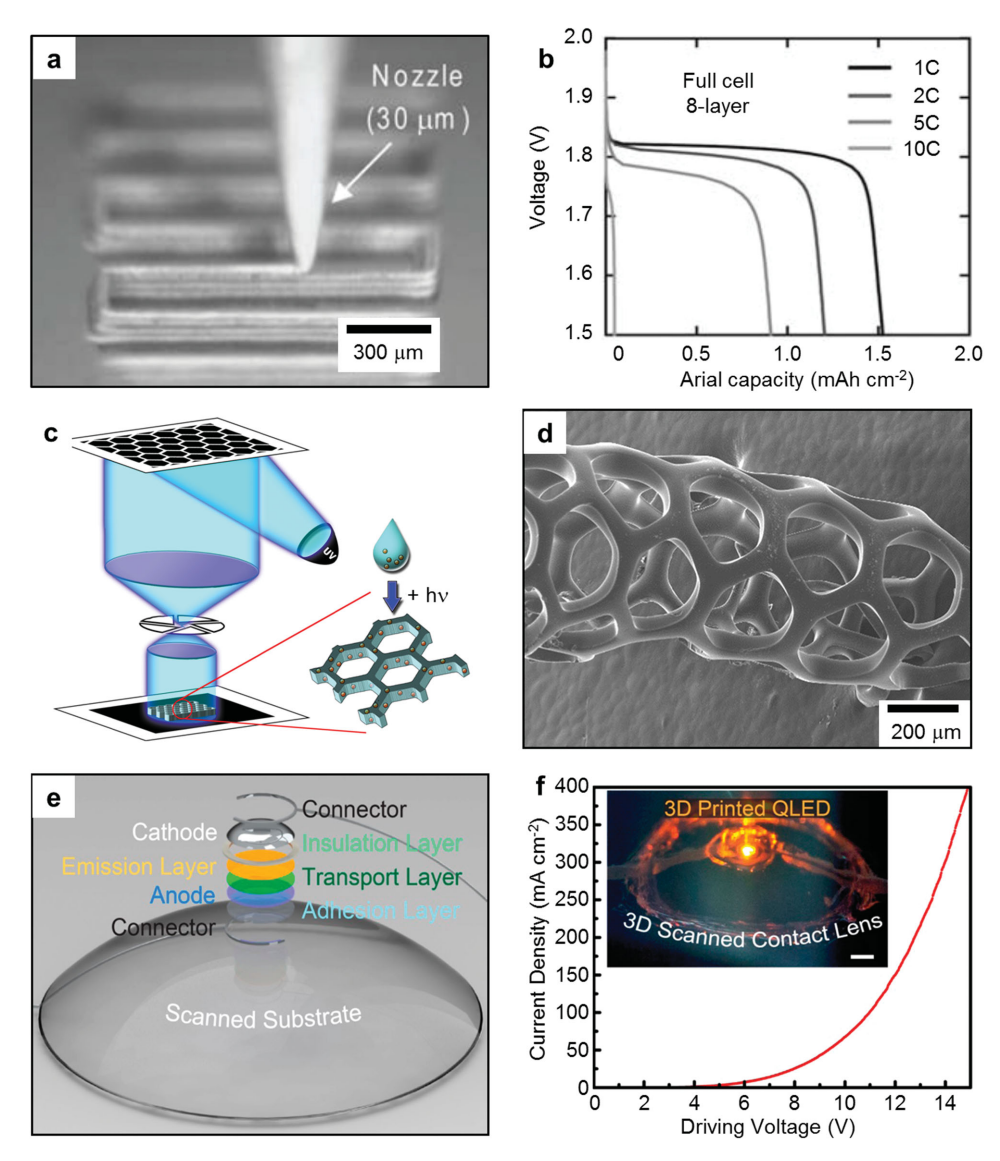


Figure 14. The three-dimensional (3D) printing method. a) Optical image of 3D-printed LiFePO₄ NC inks for a vertically packed Li-ion microbattery. b) Areal capacity versus full-cell voltage for 8-layer stacked LTO-LFP electrodes. c) A schematic of a microscale digital projection printing setup, which enables the 3D printing of microstructures made of NP/polymer composite materials. It projects dynamic digital masks on photolabile piezoelectric NP/polymer composite solutions. Any pattern can be digitized, and the digital mirror device projects the image onto the solution. d) An image of a microtubule structure formed by releasing a honeycomb array via the digital projection printing method. The structure is made of 3-trimethoxysilyl-propyl-methacrylate-passivated barium titanate (BaTiO₃) NPs/poly(ethylene glycol) diacrylate composites. e) A schematic showing 3D-printed QLEDs on a curvilinear substrate. f) Current density versus voltage (J–V) characteristics of the 3D-printed QD LEDs on top of a 3D scanned contact lens. The inset shows a photograph of the 3D-printed QLEDs during operation. The scale bars represent 1 mm. a,b) Reproduced with permission. [164] Copyright 2014, American Chemical Society. e,f) Reproduced with permission. [169] Copyright 2014, American Chemical Society.

NW films.^[183–186] **Table 3** summarizes recently reported Agbased transparent electrodes. For example, micro-Ag flakes have been mixed with Ag NWs to improve the conductivity, and graphene flakes were introduced to connect the junctions.^[187,188] Park and co-workers suggested a graphene–metal NW hybrid structure for transparent and stretchable electrodes (Figure 15d).^[179] High-density Ag NWs were sandwiched between graphene layers. This hybrid electrode exhibited a synergetic performance enhancement in terms of mechanical flexibility, high conductivity, and uniform resistance. A graphene film also prevents the oxidation of the Ag NWs. The

resulting hybrid electrode, together with inorganic LEDs on a contact lens, was applied on a rabbit's eye (Figure 15e,f). Recently, various Ag-NW–polymer composites, including Ag-NW–PEDOT:PSS,^[189] Ag-NW–TiO₂–poly(3,4-ethylenedioxythiophene:poly(styrenesulfonate) (PEDOT:PSS),^[190] Ag-NW–polyvinylpyrrolidone (PVP),^[191] Ag-NW–PVP,^[192] and Ag-NW–acrylate, have been reported.^[193] Pei's group reported a Ag-NW–polymer composite electrode.^[194,195] By controlling the mixing ratio of the Ag NWs, acrylate monomer, and crosslinker, the stretchability of the composite electrodes could be increased by as much as ca. 150%.



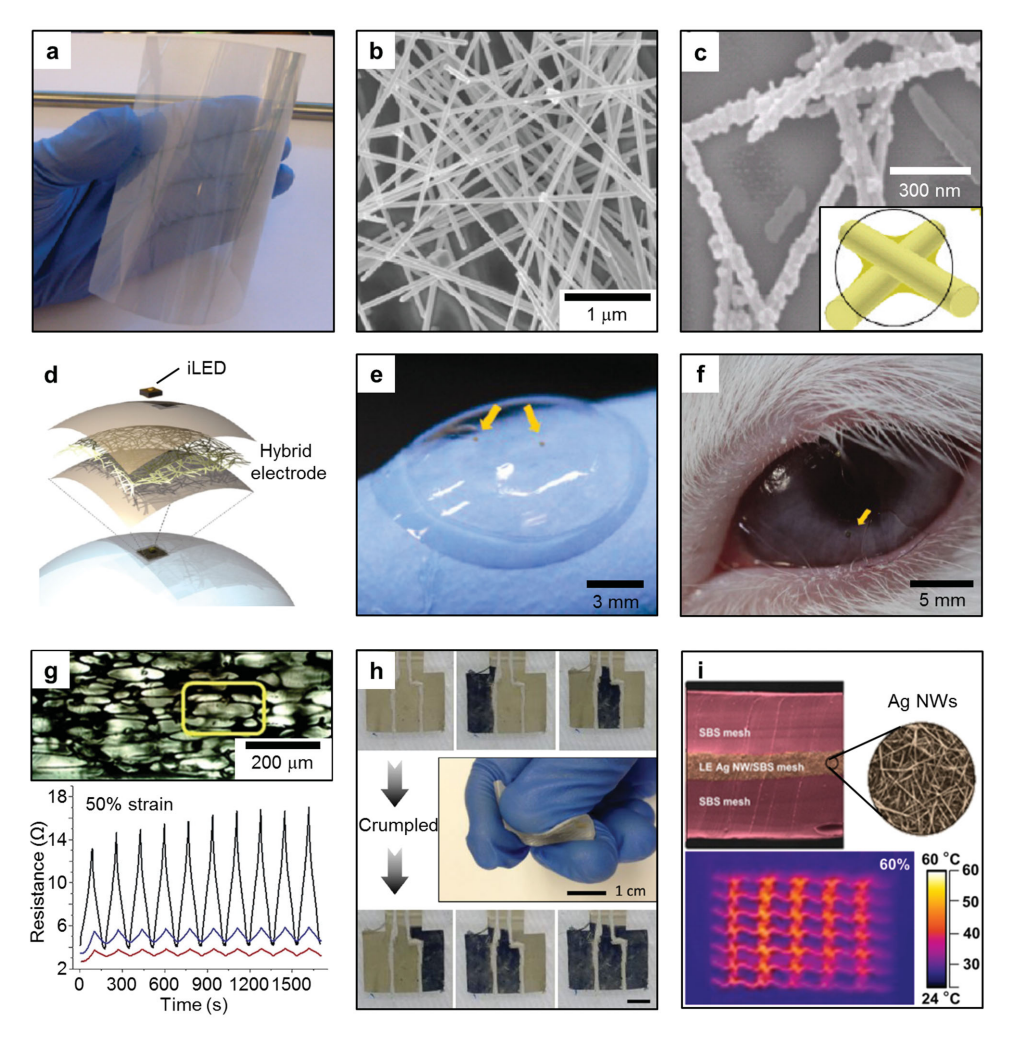


Figure 15. Conductors based on colloidal NCs. a) A photograph showing a Ag NW film coated on a PET substrate. The Ag NW film is very uniform over the entire substrate. b) An SEM image of the Ag NW film shown in panel (a). The sheet resistance of the film is 50 Ω sq⁻¹. c) An SEM image of the Ag NW film after formation of an Au-Ag alloy network by a galvanic displacement reaction. The inset is a schematic of the Au-Ag alloy network. d) A schematic illustration of a single-pixel contact-lens display employing an inorganic LED and a Ag NW/graphene hybrid electrode. e) A photograph of the contact-lens device described in panel (d). The scale bar represents 3 mm. f) A photograph of the contact-lens device on the eye of a rabbit. The scale bar represents 5 mm. g) Optical image of the 2D networked PUS-Ag-NWs-PDMS composites for the 3D stretchable conductor (top). Change in resistance under continuous applied 50% strain (bottom). Red: PUS-Ag-NWs-PDMS, blue: PUS-Ag-NWs, and black: Ag-NWs-PDMS film. h) Stretchable electrochromic devices using Ag NW electrodes. i) Cross-sectional SEM image of a Ag-NW-based thermal actuator (top) and IR camera image of the stretchable heater at 0.75 V applied voltage under a 60% stretching condition (bottom). a–c) Reproduced with permission. [178] Copyright 2010, American Chemical Society. d–f) Reproduced with permission. Copyright 2013, American Chemical Society. g) Reproduced with permission. Reproduced with permission. Reproduced with permission. Copyright 2014, American Chemical Society. Reproduced with permission. Copyright 2015, American Chemical Society.

An additional important fabrication process is inkjet printing using conductive inks that are usually composed of concentrated Ag NCs solutions. By controlling the type and ratio of NCs, surfactants, stabilizers, and solvents, various patterns with controlled electrical properties could be formed on different substrates. Krebs' group reported transparent Ag grid electrodes using the roll-to-roll printing of Ag NC inks.^[130] This pattern is potentially applicable to touch sensors. The same NC ink was applied to fabricate interconnections in unconventional macroelectronics. The NC inks were printed on substrates with various surface energies from hydrophilic to superhydrophobic, curvilinear surfaces^[196] with concave to convex structures, and 3D structured surfaces.^[145] The interconnecting electrodes were demonstrated for antennas on 3D

bowl structures, as described above, and as 3D interconnections for electronic circuits.

Another application of metallic colloidal nanocrystals and/or nanowires is their use as stretchable electronic conductors.[197] Figure 15g shows optical images of binary-networked structures of polyurethane sponge (PUS)-Ag NWs-PDMS for 3D stretchable conductors.[180] These Ag-NW-based composites show five times smaller resistance change than the Ag-NW-PDMS film in a continuous stretching test (ca. 50% applied strain) because the porous PUS acts as a 3D connected skeleton that supports the Ag-NW network. Another example is stretchable and wearable WO3 electrochromic devices demonstrated with Ag-NW conductors (Figure 15h).[181] The robust mechanical strength resulting from the Ag-NW network enables WO3 electrochromic

ADVANCED MATERIALS

www.advmat.de

Table 3. Comparison of NC-based transparent electrodes.

Conductor structure	Printing methods	Transparency (at wavelength)	Sheet resistance	Applications	Reference
PET/Ag NW	Mayer rod coating	ca. 80% (vis)	20 Ω sq ⁻¹	Flexible OLED	[178]
PET/Ag NW-PVA	Ag NW: Vacuum filtration & transfer printing	87.5% (550 nm)	$63~\Omega~\text{sq}^{-1}$	Flexible LED	[192]
	PVA: Spin casting				
Ag NW–TiO ₂ –PEDOT:PSS	Ag NW: Mayer rod coating	84% (550 nm)	$5.5~\Omega~\text{sq}^{-1}$	LED	[190]
	TiO ₂ : Spin casting				
	PEDOT:PSS: Spin casting				
Ag NW-polyacrylate	Ag NW: Drop casting Polyacrylate: Drop casting & UV curing	82% (550 nm)	$12~\Omega~\text{sq}^{-1}$	Flexible PLED	[194]
Ag NW-polyacrylate	Ag NW: Drop casting Polyacrylate: Drop casting & UV curing	86% (550 nm)	$35~\Omega~\text{sq}^{-1}$	Flexible PLED	[193]
PDMS/Ag NW	Vacuum filtration & transfer printing	90–96%	9–70 Ω sq ⁻¹	Flexible LED	[177]
Graphene Oxide/Ag NW/PET	Ag NW: Bar coating GO: Spray coating	92% (550 nm)	24.8 Ω sq ⁻¹	Flexible displays and solar cells	[188]
Graphene Oxide/Ag NW/ PDMS-Si(NNH ₂)	Ag NW: Spin casting GO: Spin casting	87% (550 nm)	27 Ω sq $^{-1}$	Stretchable and wearable solar cells, flexible displays	[187]

devices to be deformed in 3D while maintaining the fast coloration time and cyclic stability. Furthermore, nanomaterial-based conductors can be utilized as wearable thermal actuators. [182,196] Ag-NW-coated textiles prevent heat loss by reflecting IR radiation from the human body and provide thermal actuations by Joule heating. The combination of serpentine-mesh structures and styrene-butadiene-styrene (SBS)–Ag-NW nanocomposites show a stable Joule heating property under the condition of 60% stretching (Figure 15i). Recent Ag-NW-based stretchable conductors are summarized in Table 4.

4.2. Light-Emitting Diodes

Light-emitting diodes (LEDs) are emerging optoelectronic devices because of their high luminous efficacy and brightness. Semiconductor colloidal NCs have been widely studied for device elements in LEDs, such as the color filter, the emitting layer, and the electron-transport layer.[32] The application of QD films on the backlight units (BLUs) for high color purity in displays is currently commercialized. In commercial LCD displays, BLUs based on conventional white LEDs can only produce a color gamut of less than 70% of the color standard set by the National Television System Committee (NTSC). To realize natural, vivid colors, QD films have been inserted into the BLUs of displays. The NCs are usually mixed with polymers and cast on commercial blue LEDs as color filters or color converters.[198-202] The blue light from a commercial LED chip is down-converted to a longer wavelength as it passes through the NCs embedded in the polymer composite layer (Figure 16a). The unique properties of QDs, such as the easy color tunability, narrow emission spectra, and high

luminescence efficiency, efficiently realize tunable, reproducible colors. Figure 16b shows active-matrix LEDs with QD color filters. [203] Many companies have applied QD layers in their displays. For example, QD Vision developed QD-based color filters and applied them in LCD displays; in these applications, color gamuts of nearly 100% of the color standard were achieved.

Another important application of QDs for lighting devices and displays includes the EL devices.[73,204-207] QD films have been employed as emissive electroluminescent layers in QLEDs.^[208] The first QLEDs were reported by Alivisatos's group in 1994 using spin-cast CdSe NCs with a p-phenylene vinylene hole-injecting layer. [209] QDs are typically spin-cast and sandwiched between the hole-transport layer (HTL) and the electron-transport layer (ETL). When the external voltage is biased, electrons and holes are injected from the ETL and HTL layers, respectively. The electron-hole pair is recombined in the QD layer, emitting photons with an energy corresponding to the bandgap of the core NCs. Figure 16c shows a typical band diagram for QLEDs. Generally, thin films of core/ shell-type QDs such as CdSe/ZnS,^[210] CdSe/ZnSeS,^[211,212] and InP/ZnSeS^[213,214] have been used as emitting layers. Core/ shell-structured NCs are beneficial to QLEDs because the thick shells effectively confine the charge-carrier wave function and protect the core NCs from oxidation.^[215,216] The thickness of the QD layer must be carefully modulated to match effective charge recombination in the QD layer. Lee and co-workers reported that a QD film thickness five times thicker than that of the QD monolayer is the optimum. QLEDs with a QD monolayer show low efficiency due to the leakage current through NC vacancies, while QLEDs with QDs of 6 layers or higher show a low current density and thereby a low brightness. [217]

Table 4. Comparison of NW-based stretchable conductors.

Conductor structure ^{a)}	Printing method	Stretchability	Resistance or conductance	Applications	Reference
AgNW–PDMS	Lithographic filtration	50%	4.5 Ω	Wearable ECD	[181]
PUS-AgNW-PDMS	Dip coating	50%	19.2 S cm ⁻¹	Stretchable conductor	[180]
AgNW–PDMS	Casting	50%	5285 S cm ⁻¹	Stretchable conductor	[197]
SBS-AgNW-SBS	Casting	100%	0.8 Ω	Wearable heater	[182]
AgNW-PVP	Dip coating	-	_	Wearable heater	[196]

a) PUS: polyurethane sponge.

The exciton-recombination zone within the QD multilayers was systematically analyzed with QD films assembled by the layer-by-layer spin-casting process. Moreover, by optimizing the conduction- and valence-band energy levels of the HTL and ETL, highly effective QLEDs can be achieved.^[218] Various semiconductor materials such as organic molecules, polymers. and inorganic materials have been employed as charge-transport layers. Conducting polymers and inorganic NPs are commonly used as the HTL and ETL, respectively. More recently, ZnO NCs have been used as the electron-transport layer due to their intrinsically high conductance and optical transmittance. [219] In the QLED structure, a uniform NC layer with precisely controlled thickness is important because the HTL, EL, and ETL layers must be stacked as discrete films, but have high-quality interfaces with minimum defects, to enhance the luminance efficiency. A recently reported film-fabrication process, the microcontact printing of a dry QD layer, has many merits.[220] It prevents the penetration of QDs and the organic solvent into the underlying HTL. Moreover, a transfer-printed QD layer attains a more-compact film density than a spin-cast QD layer.[160]

The applications of QLEDs can be classified into two major categories: white QLEDs for backlight or lighting devices and multicolor QLEDs for full-color displays.[221] To realize co-planar multicolor QD patterns, microcontact printing and inkjet printing have been utilized. The most widely used process for white QLEDs is the spin casting of mixed RGB QDs.[222] The emitting layer consists of randomly mixed RGB QDs. In this structure, however, interparticle energy transfer occurs from B to G and R, and from G to R, which decreases the internal quantum efficiency.[70,223] To reduce the energy transfer, multistacked OD monolayers using transfer printing were introduced. In this approach, a blue monolayer was placed between the red and green monolayers. The B/G/B/R sequence of the QD stacks effectively prohibits energy transfer from G to R, and presents a pure white emission. Extending this idea, Kim, Hyeon, and co-workers reported pixilated, flexible white LEDs with aligned RGB pixels (Figure 16d).[141] As the RGB pixels were spatially separated, there was no energy transfer between QDs of different colors. Consequently, the luminance of the pixelated white QLEDs was enhanced by about 10% over that of the mixed white QLEDs.

Recently, deformable multicolor QLED arrays have received tremendous attention for next-generation displays. Microcontact printing is a powerful tool for realizing coplanar RGB QD patterns. Samsung manufactured an active-matrix, full-color QD display on a flexible substrate. [160] To realize multicolor

displays, RGB QDs were spatially patterned using a structured elastomer stamp. Figure 16e shows an EL image of a 4-inch QLED with a 320×240 pixel array. Kim, Hyeon, and

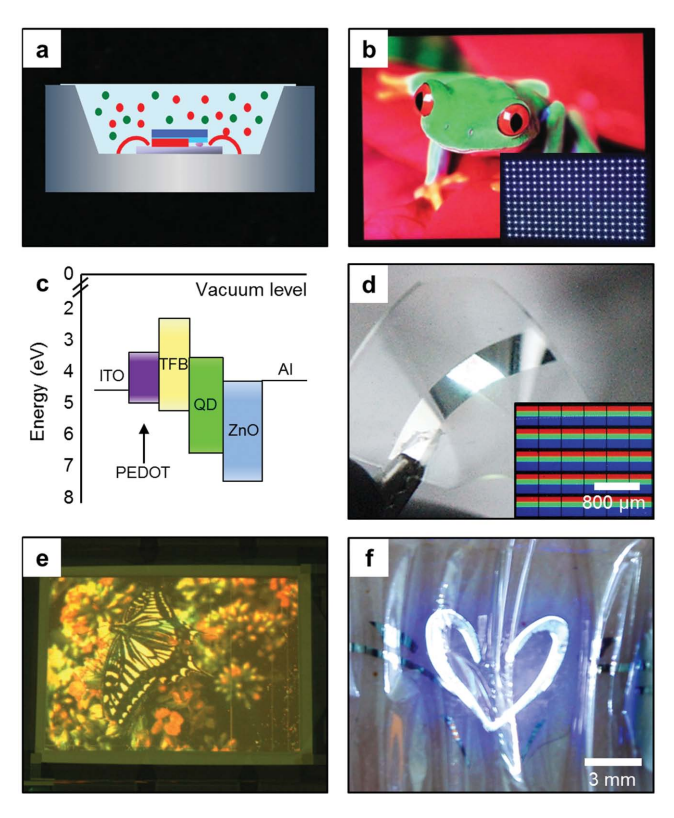


Figure 16. Light-emitting diodes using colloidal NCs. a) A schematic showing the side view of the QLED; QDs (red and green dots) are encapsulated in a silicone resin and used as color converters for the blue LEDs to produce white light. b) A photograph of a 46-inch liquid-crystal display (LCD) television panel using the white QLEDs shown in (a). The inset shows the white QLED backlights. c) Energy-band diagram of white QLEDs fabricated by the intaglio transfer-printing process. The energy levels were estimated by ultraviolet photoelectron spectrometry. d) An optical image of operating flexible white QLEDs fabricated by the intaglio transfer-printing process. The bending radius is 1 cm. The inset shows a magnified view of the RGB QD pixels. e) A photograph showing the electroluminescence from a 4-inch fullcolor QD display using a hafnium-indium-zinc-oxide thin-film transistor backplane with a 320×240 pixel array. RGB QD layers were printed by the subtractive transfer printing. f) A photograph showing wearable blue QLEDs laminated on uman skin. The device maintains the performance under deformation. a,b) Reproduced with permission. [203] c,d,f) Reproduced with permission.^[41] Copyright 2015, Nature Publishing Group. e) Reproduced with permission.[160] Copyright 2011, Nature Publishing Group.



ADVANCED MATERIALS

www.advmat.de

www.MaterialsViews.com

co-workers reported a high-resolution transfer-printing technique achieving an ultrahigh resolution of the RGB QD patterns (2460 pixels per inch) without any deformation of the pattern features. [41] Moreover, with this technique, they demonstrated an ultraflexible electronic tattoo, skin-mounted QLEDs (Figure 16f) that operated in ambient air or wet conditions. The electronic tattoo exhibited high brightness (14 000 cd m⁻² at 7 V bias) and an external quantum efficiency (EQE) of 2.35% at a 4.5 V bias. Table 5 provides a summary of QLEDs reported in recent years. Different NC materials and device designs have been studied to increase the EQE and brightness.

4.3. Solar Cells

NC-based-solar cells have been considered as next-generation energy-harvesting devices due largely to the novel optoelectrical properties of semiconductor NCs and their cost-effective fabrication processes. [224–226] QD solar cells can be categorized into four different types: QD-sensitized solar cells (QDSSCs), Schottky solar cells, depleted heterojunction solar cells, and hybrid NC-polymer solar cells. Figure 17a shows schematic illustrations of each type. The representative device structures, process conditions (deposition method, pre-/post-ligand-exchange, etc.), and optoelectronic characteristics of each type of solar cells are compared and summarized in Table 6 and Table 7.

A QDSSC comprises a nanoporous electrode containing the semiconductor NCs, a redox-coupling electrolyte, and a counter electrode. The NCs play two different roles as nanostructured electrodes and light-absorbing sensitizers. TiO2 NCs are commonly employed as an electrode to increase the interfacial area for effective charge transport. [229] Anatase TiO2 NCs are spread on the transparent electrode by doctor-blading or screenprinting techniques, and then sintered to form a nanoporous TiO₂ electrode (Figure 17b).^[108] Semiconductor NCs, which act as photosensitizers, are drop-cast and then smeared into the pores of the TiO₂ electrodes. The NCs absorb visible light, inject photogenerated electrons to the TiO2 electrode, and are reduced by the infiltrated electrolyte. Nozik's group first reported InP-QD-based QDSSCs in 1998. [227] QDSSCs have attracted great attention because of the unique properties of the NCs, such as their size-tunable absorption energy levels, sharp absorption onsets, and large absorption coefficients. Recently, Zhong and co-workers reported a photoconversion efficiency (PCE) of 8.55% with CdTe_{1-x}Se_x QDs.^[230] Furthermore, Hyeon and coworkers demonstrated heavy-metal-free Cu-In-Se QDSSCs with PCE of 8.10%. [245]

NC-based Schottky solar cells, which have the simplest structures, were reported by Sargent's and Nozik's groups. [231–234,246] Densely packed, monodisperse semiconductor NCs (PbS and PbSe[231] were utilized as the light-absorbing semiconductor layer and sandwiched between ITO and a reflective metal electrode (Al,[232] Mg,[233] and Ca/Al[234] (Figure 17c). Because of their simple architecture, the distinct characteristics of colloidal NCs can be fully utilized in Schottky solar cells. During their synthesis, the NCs are capped with long-chain organic ligands (e.g., oleic acid, oleylamine, trioctylphosphine oxide (TOPO)) to enhance their dispersibility and stability, but the ligands

act as insulators, which leads to very poor interparticle carrier transport. To increase carrier mobility, these long-chain NC ligands are exchanged with short-chain ligands. The spin-cast NC layer is immersed in a solution of a short-chain surfactant (e.g., ethanedithiol or butylamine) to form densely packed NC layers, but only ligands exposed on the surface are exchanged because of the inefficient diffusion.^[234] Sequential layer-by-layer spin casting of NC monolayers and short-chain surfactants creates a dense NC layer with few defect sites. The Schottky barrier forms at the interface between the metal and semiconductor NC layer, and the photogenerated majority carriers are separated in the depletion region and diffuse to the negative electrode. Law's group reported the effects of the NC sizes and solid-state ligand exchange (i.e., short-chain acids, diacids, [247] or dithiols^[248] on the charge mobility. When the NCs (PbS and CdTe) were capped with double-ended thiol groups, which effectively passivate the NC surfaces, the electron and hole mobilities were inversely proportional to the ligand length. By optimizing the size of the NCs, Nozik's group reported a PCE of 4.5% with simple Schottky structures.^[249]

Depleted heterojunction (DH) QD solar cells have been developed to take advantage of QDSCs and Schottky solar cells. The DH design, with the transparent electron-accepting layer, benefits from minority-carrier separation due to the placement of the junction on the illuminated side. Moreover, the multilayer structure of the absorbing NC film increases the absorption coefficient and the current density. [237] A dense and conformal film of a transparent conducting oxide with a wide bandgap (TiO2 or ZnO), which acts as an electron acceptor, is deposited on the transparent electrode. Subsequently, semiconductor NCs with shallow bandgaps (i.e., PbS and PbSe) are spin-cast to a thickness of 50–300 nm (Figure 17d). [243] The thickness of the NC film must be optimized for high-efficiency cells. A film that is too thin is insufficient to fully absorb the incident light, whereas a thick film decreases the current density due to the short depletion length. Sargent's group suggested mercaptopropionic acid as a short-chain organic crosslinker in DH solar cells. [235,237] They discovered that a bandgap for the NCs of greater than 0.9 V is desirable to lower the electroninjection barrier between the PbS NCs and TiO2. Solid-state ligand exchange was performed on the precoated QD layer. The thiols completely displaced the long aliphatic ligands, which increased the current density and efficiency. [225] The size of the photosensitive NCs is also critical for managing the oxide/NCs junction.[228,250] Bulović, Bawendi, and co-workers reported an improved performance and stability in QD solar cells through band alignment engineering.^[226] Double-layered different ligand treatments of PbS QD solar cells show high efficiency of 8.55% and durability of 150 days without encapsulation. Additional detailed information about QD solar cells can be found in a recent review paper by Sargent. [251]

Hybrid NC–polymer solar cells were proposed to solve the problems in polymer solar cells, such as the chemical-/photoinstability of the organic materials, the poor electron mobility of the ETL layer (ca. 1000 times smaller than the hole mobility of the HTL), and the wide bandgap of the active polymer layer. Semiconductor NCs (e.g., CdSe,^[252] CdS,^[253] CuInSe₂,^[254] HgTe,^[240] PbS,^[242,255] and PbSe^[238]) have been utilized as the photosensitive layer to extend the absorption range



Table 5. Comparison of the LED performance.

QD material	Printing method	Information re. NC solution	Device structure	Max. Luminance	EL color ^{a)}	EQE ^{b)}	Ref.
CdSe	Spin casting		ITO/QDs/PPV/Mg	-	G to R	0.001-0.01	[209]
CdSe/ZnS	Spin casting (monolayer)	Toluene, alkanes, chloroform (10 mg mL ⁻¹)	ITO/TPD/QDs/Alq3/Mg:Ag/Ag	2000	-	ca. 0.52	[73]
$Cd_xZn_{1-x}Se/Cd_yZn_{1-y}S$	Microcontact printing (monolayer)	-	ITO/CBP/QD(monolayer)/TAZ// Alq3/Mg:Ag/Ag	-	G	<0.5	[220]
CdSe/CdS	Spin casting (1000 rpm)	Toluene	ITO/PEDOT/polyTPD/QD/Alq3/ Ca/Al	3200	Orange	-	[206]
CdSe/ZnS	Spin casting (1.1 monolayers)	Chloroform	ITO/PEDOT:PSS/TPD/ QD(monolayer)/TAZ/Alq3/Mg/Ag	100	White	ca. 0.36	[222]
ZnCdSe	Spin casting	Chloroform	ITO/NiO/QDs/ZnO:SnO ₂ /Ag	1950	R	ca. 0.1	[205]
ZnCdS	Contact printing (monolayer)	Chloroform	ITO/PEDOT:PSS/spiroTPD/TPBi/ Mg:Ag/Ag	15	R, G, B	1.0, 2.6, 0.4	[208]
CdSe/CdS/ZnS	Spin casting (2000 rpm 30s)	Cyclohexane (10 mg mL ⁻¹)	ITO/PEDOT:PSS/TFB/QD/TiO ₂ /Al	12 380	R	2.41 lm W ⁻¹	[210]
CdSe/ZnS	LBL spin casting (4000 rpm, 30 s)	water	ITO/PAH/QD-MPA, QD-Cam/TPBi/ LiF-Al	1000	R, orange, G	0.3	[217]
CdSe/CdS/ZnS	Transfer printing (30 nm thick)	cyclohexane	ITO/PEDOT:PSS/polyTPD/QD/ TiO ₂ /Al	16 380 (R), 6425 (G), 423 (B)	R, G, B	4.25 lm W ⁻¹ (R)	[160]
CdSe/ZnS	Spin casting (500–2000 rpm)	Toluene (10 mg mL ⁻¹)	ITO/PEDOT:PSS/polyTPD/QD/ ZnO/Al	31 000 (R), 68 000 (G), 4200 (B)	R, G, B	1.7, 1.8, 0.22	[219]
ZnCuInS/ZnS	Casting (ca. 7 nm)	Toluene	ITO/PEDOT:PSS/polyTPD/QD/Al	450 (16V)	White	0.033	[221]
CdSe/CdS/ZnS(R), CdSe@ZnS(G), $Cd_{1-x}Zn_xS@ZnS(B)$	Spin casting (4000 rpm, ca. 2 monolayers)	Toluene (20 mg mL ⁻¹)	ITO/ZnO//QD/CBP/MoO ₃ /Al	23 040 (R), 218 800 (G), 2250 (B)	R, G, B	7.3, 5.8, 1.7	[212]
CdSe/CdS	Spin casting (2000 rpm)	Hexane	ITO/ZnO/QD/NBP/HIL/Al	>50 000	Red	18	[218]
CdSe/CdS/ZnS	Transfer printing	Cyclohexane	ITO/PEDOT:PSS/TFB/QD/TiO ₂ /Al	1040 (10 V)	White	-	[70]
CdSe/CdSe _{0.5} S _{0.5} /CdS	Spin casting (4000 rpm)	Hexane (15 mg mL ⁻¹)	ITO/ZnO/QD/CBP/MoO _x /Al	>7000 (>7 V)	Red	1.8	[215]
CdSe/CdS	Spin casting	Octane (15 mg mL ⁻¹)	ITO/PEDOT:PSS/polyTPD/PVK/ QDs/PMMA/ZnO/Ag	>42 000 (8 V)	Red	20.5	[204]
$CdSe/Cd_{1-x}Zn_xSe_{1-y}S_y/ZnS$	Spin casting (2000 rpm, ca. 20 nm)	Toluene (18 mg mL ⁻¹)	ITO/PEDOT:PSS/TFB/QD/ZnO/Al	R: 21 000 (3.5 V), G: 14 000 (4 V), B: 4000 (6 V)	R, G, B	12, 14.5, 10.7	[216]
CdSe/ZnS	Transfer printing (40 nm thick)	Cyclohexane	ITO/PEDOT:PSS/TFB/QD/ZnO/LiAl	14 000 (7 V)	R, G, B	2.35	[41]

 $^{^{}a)}R = red, G = green, B = blue; ^{b)}EQE$: external quantum efficiency.

and to increase the electron mobility. The NCs and conductive polymers (donor and accepter) are blended to improve the charge-separation interfaces (bulk heterojunction). The percolated interfaces of p-type and n-type regions effectively transfer the photogenerated charges to the electrodes. The first hybrid bulk heterojunction solar cells were reported by Alivisatos's group in 2002 using blends of poly(3-hexylthiophene-2,5-diyl) (P3HT) and shape-controlled CdSe NCs (dots and rods). [256] The 1D rod structures show the higher light-conversion efficiency than 0D dot structures because 1D rod structures decrease interparticle hopping events of electrons and improve charge collection. However, as the nanorods tend to align in parallel to the substrate, the photogenerated electrons are inefficiently collected. Thus, branched nanocrystals such as tripods and

tetrapods were blended with the polymer layer to improve electron transport and prevent phase separation in the NC-polymer hybrid layer (Figure 17e).[239,241,244]

4.4. Photodetectors

Colloidal QDs are attractive candidates as active materials for photodetectors, especially in the infrared spectral range. In the visible-light spectral range, there are well-established detection systems, such as charge-coupled devices, photodiodes, photoresistors, and photomultiplier tubes. Many high-performance photodetectors are based on silicon technologies, but silicon cannot absorb infrared light. Other compound semiconductors





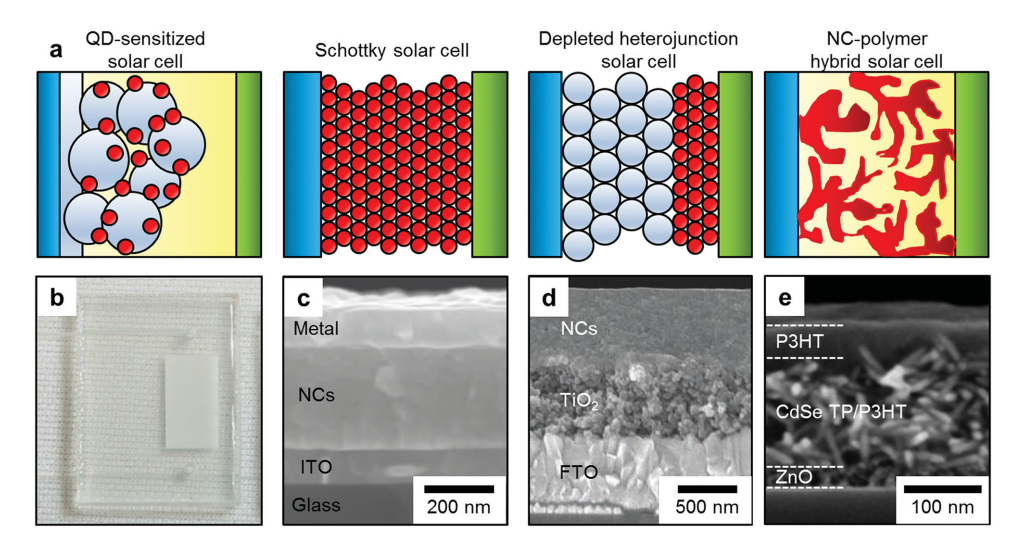


Figure 17. Colloidal NCs in solar cells. a) Schematics showing the four representative types of QD solar cells: the quantum-dot-sensitized solar cell, the Schottky solar cell, the depleted-heterojunction solar cell, and the NC-polymer hybrid solar cell. b) A photograph of the bare TiO₂ NC layer in a quantum-dot-sensitized solar cell, which was deposited by the doctor-blading method. c) An SEM cross-sectional image of the ITO/NC film/metal device stack of a PbSe NC Schottky solar cell. The scale bar represents 100 nm. d) An SEM cross-sectional image of the NC film stack of a PbS solar cell. e) An SEM cross-sectional image of the blend of CdSe tri-/tetra-pods and P3HT for the bulk-heterojunction solar cell. b) Reproduced with permission.^[108] Copyright 2013, Royal Chemical Society. c) Reproduced with permission.^[232] Copyright 2008, American Chemical Society. d) Reproduced with permission.^[244] e) Reproduced with permission.^[244] Copyright 2014, American Chemical Society.

Table 6. Comparison of the solar-cell performance.

Type of solar cell	QD material	Printing method	Information of NC solution	Ligand ^{a)}	Device structure	^{b)} PCE ^{c)} [%]	Reference
QDSSC	InP	Dip coating	Toluene	ТВР	TiO ₂ /NC	Very low	[227]
QDSSC	PbS	Dip coating	Toluene	-	FTO/TiO ₂ +NC/Pt	0.28	[228]
QDSSC	CdSeTe	Dip coating	-	_	TiO ₂ /NC/Cobalt complex	4	[229]
QDSSC	CISe	Dip coating	Dichloromethane	Oleic acid	FTO/TiO ₂ /NC	4.3	[108]
QDSSC	CdSeTe, CdSe	Dip coating	Water	TGA	FTO/TiO ₂ + ZnS,SiO ₂ /NC	8.21	[230]
Schottky	PbSe	Spin coating	Octane (80 mg mL ⁻¹)	Benzenedithiol	ITO/NC/Mg	3.6	[231]
Schottky	PbSe	Dip coating	Hexane	Oleic acid	ITO/NC/Metal	2.1	[232]
Schottky	PbSe	Dip coating	Octane (150 mg mL $^{-1}$)	n-butylamine	ITO/NC/Mg	2	[233]
Schottky	PbSe	Dip coating	Hexane (4 mg mL ⁻¹)	EDT	ITO/NC/Ca/Al	60 (EQE)	[234]
DH	PbS	Spin casting (2500 rpm)	Octane:decane = $3:1$ (37.5 mg mL ⁻¹)	MPA	SnO ₂ :F/TiO ₂ /NC/Au	5.1	[235]
DH	PbS	LBL spin casting (2500 rpm)	Octane (50 mg mL ⁻¹)	MPA	FTO/TiO ₂ /ZnO/NC/ MoO _x /Au/Ag	7.4	[225]
DH	PbS	Spin casting (2500 rpm)	Octane (50 mg mL ⁻¹)	TBAI, EDT	ITO/ZnO/NC/ electrode	8.55	[226]
DH	PbSe	Dip coating	Hexane (20 mg L ⁻¹)	EDT	ITO/ZnO/ PbSe/α-NPD/Au	2	[141]
DH	PbS	LBL spin casting (2500 rpm, 10s, 200 nm thick)	Octane (25 mg mL ⁻¹)	МРА	ITO/TiO2/PbS/GRL/ PbS/Au	4.2	[237]

^{a)}TBP: 4-tertbutylpyridine, TGA: thioglycolic acid, EDT: ethanedithiol, MPA: mercaptopropionic acid, TBAI: tetrabutylammonium iodide; ^{b)}GRL: graded recombination layer (MoO_x/ITO/AZO/TiO₂); ^{c)}PCE: photoconversion efficiency.

Adv. Mater. 2016, 28, 1176-1207



Table 7. Comparison of the NC-polymer hybrid solar-cell performance.

QD material	Printing method	Information of NC solution	Ligand ^{a)}	Blended polymers ^{b)}	Device structure	PCE ^{c)} [%]	Reference
CdSe NR + P3HT	Spin casting (200 nm thick)	Pyridine-chloroform	TDPA	P3HT	ITO/PEDOT:PSS/ CdSe+P3HT/Al	1.7	[238]
CdSe tetrapod + OC ₁ C ₁₀ -PPV	Spin casting (160–180 nm thick)	Pyridine:chloroform = 1:9 (50 mg mL ⁻¹)	Pyridine	OC ₁ C ₁₀ -PPV	ITO/PEDOT:PSS/ CdSe+OC ₁ C ₁₀ -PPV/ Al	4.5	[239]
PbS + MEH-PPV	Spin casting (100–150 nm thick)	Chloroform	octylamine	MEH-PPV	ITO/PPV/ NC+MEH-PPV/Mg	-	[224]
HgTe	Drop casting	Chlorobenzene	Thioglycerol	P3HT	ITO/TiO ₂ /NP-TiO ₂ / P3HT/Au	0.4	[240]
CdSe NR/ branch+P3HT	Spin casting (1500 rpm)	Pyridine:chloroform = 1:9	TDPA	P3HT	ITO/CdSe+P3HT/Al	2.2	[241]
PbS + P3HT	Spin casting (8000 rpm)	Ethyl acetate:chloroform = 1:6	Oleic acid	P3HT	ITO/PbS/P3HT/Au	0.02	[242]

a)TDPA: Tetradecylphosphonic acid; b)P3HT: Poly(3-hexylthiophene), MEH-PPV: poly(2-methoxy-5-(2'ethyl-hexoxy)-1,4-phenylene-vinylene); c)PCE: photoconversion efficiency.

show less sensitivity or are very difficult to process. Thus, the use of QDs, which have tunable bandgaps, has been intensively pursued.

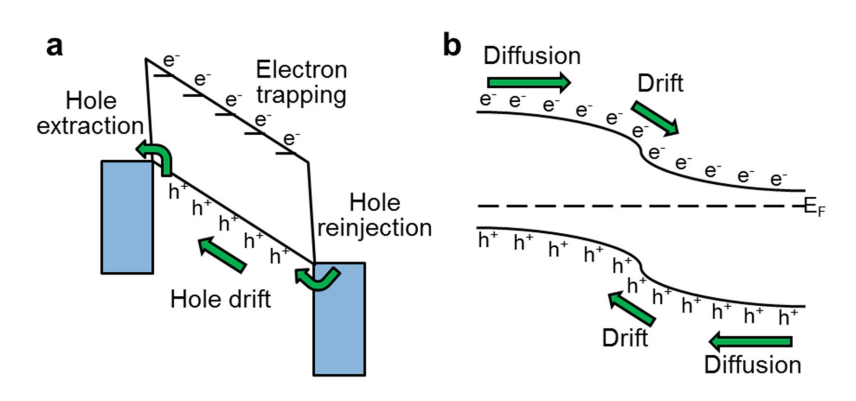
Figure 18a,b show the basic operational principles of photoconductors and photodiodes. Basically, all kinds of semiconductors can exhibit photoconductivity. The photocurrent of NC-based photodetectors can be enhanced by exchanging the ligands with shorter ligands. The first colloidal NC-based photoconductor was reported by Bawendi, Bulović, and coworkers for visible-light detection using CdSe NCs. [257] Butylamine-treated CdSe NC solids were incorporated between ITO/ PEDOT:PSS and Ag electrodes. In 2006, an impressively high performance was reported for a near-infrared photodetector by Sargent's group. [55] Butylamine-capped PbS QDs were spin-cast to obtain an NC film that was several micrometers thick. The device showed unpredictably high efficiency in terms of sensitivity (2 \times 10¹² Jones at 30 Hz), which exceeded that of commercial photodiodes using compound semiconductors. The same group subsequently reported a visible-light detector using smaller PbS QDs. [258] Siebbeles' group studied the ligand effects on the photoconductivity and charge-carrier mobility systemically by changing the chain lengths and functional groups of ligands. [81,259] PbSe QDs were dip coated using the layer-bylayer method to make dense NC solids. They demonstrated that the NC solids with amine functional groups present a higher charge-carrier mobility than thiol groups with the same chain length.[82] Heiss's group demonstrated mid-infrared photoconductors using HgTe NCs (Figure 18c).[260] The inkjet-printing process was applied to integrate dodecanethiol-capped HgTe NCs into the device. This printed photoconductor showed an extended operational range, as high as 3 µm. A heavy-metal-free photoconductor was also demonstrated by Sargent's group. [261] They used arrays of Bi₂S₃ nanorods as alternative materials for lead-, cadmium-, and mercury-based devices.

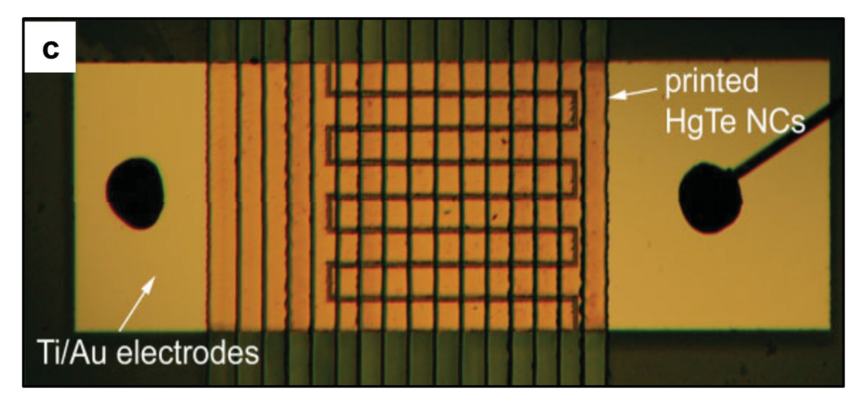
Photodiodes can have a fast response time compared to photoconductors. In this structure, the carriers move much faster in the depletion region than in the diffusion layer. Consequently, high device performance can be achieved by forming fully depleted devices with controlled NC layer thicknesses. Sargent's group reported ultrafast and sensitive infrared photodiodes using PbS NCs.^[263] The structure of the device is the Schottky type (ITO/PbS NCs/Al electrodes). The device showed a MHz response in the fully depleted photodiode while maintaining high detectivity (ca. 10¹² Jones).

Sometimes, colloidal NCs can be synergistically combined with organic/carbon materials. For example, enhanced photocurrents could be achieved by mixing visible-light-sensitive organics and narrow-gap QDs. Many combinations such as CdSe NCs and C₆₀,^[264] PbS NCs and C₆₀,^[265] and a mixture composed of CdTe NCs, [6,6]-phenyl-C61-butyric acid methyl ester (PCBM), and poly(3-hexylthiophene) (P3HT),[266] have been investigated. This strategy was successfully applied to infrared active photodiodes. [267] PbS NCs were employed with PCBM and P3HT to form a hybrid bulk heterojunction on an amorphous silicon active matrix backplane. Efficient near-infrared imaging was realized with this hybrid photodiode, as shown in Figure 18d. Similarly, colloidal NCs can be hybridized with graphene. Konstantatos et al. reported graphene/QD photofield-effect transistors (FETs), where PbS NCs absorb light and transport carriers to the highly conductive graphene. [268] Owing to the synergetic effects of the long lifetimes of the trapped carriers and the high mobility of the graphene, the device showed an excellent gain of ca. 108. The detailed solution deposition conditions of key references are summarized in Table 8.

4.5. Transistors

Semiconductor NCs have attracted tremendous attention as next-generation solution-processable building blocks for electronic devices. For instance, NC FETs can be used as basic devices for integrated circuits. By combining n- and p-type transistors, diverse electronic devices such as inverters, amplifiers, and logic gates can be realized. The representative benefits of colloidal NCs in FETs and related devices are their solution-processability over large areas, their compatibility with flexible





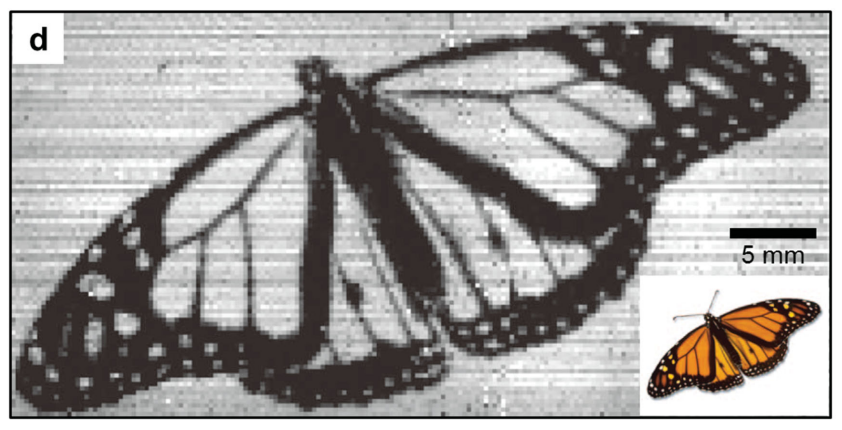


Figure 18. Photodetectors based on NCs. a) A schematic showing photoconductors. In a photoconductor, one type of carrier circulates while the other is trapped under the influence of an electric field. b) A schematic showing photodiodes. Photogenerated electron—hole pairs are separated at the p—n junction by a built-in potential. The dashed line represents the Fermi level. c) A photograph showing the photoconductors prepared with inkjet-printed HgTe NCs. The picture is a top view of the interdigitated contacts with an array of 16 printed NC stripes. d) IR shadow cast at a wavelength of 1310 nm from a slide showing a monarch butterfly acquired by PbS-NC-sensitized hybrid photodetectors. The inset shows the original slide for comparison. c) Reproduced with permission.^[260] d) Reproduced with permission. Copyright 2009, Nature Publishing Group.

and stretchable substrates, and the low cost of materials and processing.

Semiconductor NCs (i.e., CdSe, InP, PbSe, and PbS) have been used as semiconducting channel materials in transistors. Generally, the NCs are spin-cast on oxidized Si wafers. A thin SiO_2 layer (100–300 nm) and the backside Si wafer function as the gate dielectric and back gate, respectively. The source and drain metal electrodes are thermally evaporated and patterned

on the NC layer. The organic ligands on the NC surface limit charge transfer between the NCs to form an electrical barrier. To increase the carrier mobility, various kinds of ligand-exchange processes have been investigated.

The first NC-based FETs were reported in 1999 by Jacobson's group using a spin-cast pyridine-capped CdSe NC layer. [269] However, a large percentage of the NCs was severely aggregated during the high-temperature annealing process. Talapin and Murray fabricated a closely packed NC channel layer for FETs using spin-cast PbSe NCs. The initial oleic acid ligands were exchanged with hydrazine to increase mobility.[60] Nozik's group systematically studied ligand effects on the device performance. They tested various short-chain ligands that had different functional groups, such as methylamine, pyridine, and ethanedithiol.[61,80] When the capping ligands were exchanged with shortchain ligands, the overall volume of the NC layer was reduced because the interparticle distances decreased. During this volume shrinkage, voids that often function as electron sinks and defect sites were generated. To produce a highly conductive and compact NC film without these types of defects, NCs were sequentially coated and crosslinked with the ligand exchange by short-chain ligands.[270,271] The pre-coated NC layer may have had defects, including voids, after the crosslinking, but these defects/voids could be recovered by the over-coating of new NC layers.[272]

Talapin's group reported all-inorganic colloidal NCs by replacing the organic ligands with metal chalcogenide ligands (Sn₂S₆⁴⁻, $In_2Se_4^{2-}$, Ga_2Se_3 , Sb_2Se_3 , Sb_2Te_3 , $CuInSe_2$, CuIn_xGa_{1-x}Se₂, and HgSe)^[64] and metal-free inorganic ions (S2-, HS-, Se2-, HSe-, Te2-, HTe⁻, and TeS₃²⁻),^[262] which dramatically increased the interparticle carrier mobility, and thereby, the conductivity of the NC layer. These short ligands were applied to NCs of a wide range of materials including metals, semiconductors, and oxides. The same group reported metal-chalcogenide complex ligands (SnS₄⁴⁻, Sn₂S₆⁴⁻, SnTe₄⁴⁻, AsS₃³⁻, MoS₄²⁻, and In₂Se₄² that can stabilize NCs in polar media[65] and facilitate a high mobility of CdSe/CdS (16 cm² V⁻¹ s⁻¹).^[273] These all-inorganic NCs

show dramatically improved conductivities (>1000 S cm $^{-1}$). Moreover, inorganic halide, pseudohalide and halometallate ligands have been investigated to provide electrostatic stabilization of NCs and high electron mobility (ca. 12 cm 2 V $^{-1}$ s $^{-1}$). These inorganic ligand exchanges can expand latent opportunities for applications of NCs in the fields of electro-/optoelectronics.

Recently, flexible NC transistors were demonstrated by Kagan's group.^[275] Figure 19a shows a schematic image of

Table 8. Comparison of the photodetector performance.

QD material	Printing method	Information of NC solution	Ligand ^{a)}	EQE ^{b)} or responsivity	Reference
CdSe	Spin casting (200 nm thick)	Chlorobenzene	Butylamine	0.20%	[257]
PbS	Spin casting (800 nm thick)	Chlorobenzene	Butylamine	2700 A W ⁻¹	[55]
CdSe + C ₆₀	Drop casting	Toluene (30 \times 10 ⁻⁶ M)	TOPO/TOP	ca. 10%	[264]
PbS	Spin casting (360 nm thick)	Toluene	Butylamine	120 A W ⁻¹	[258]
HgTe	Inkjet printing (100 nm thick)	Chlorobenzene (2 wt%)	Dodecanethiol	4.4 A W ⁻¹	[260]
Bi_2S_3	Spin casting (120 nm thick)	Toluene	Ethanthiol	20 A W ⁻¹	[261]
CdTe + P3HT + PCBM	Spin casting (800rpm 95s)	Dichlorobenzene (380 mg mL ⁻¹)	PMDTC	50 A W ⁻¹	[266]
PbS	Spin casting (350 nm thick)	Octane	Benzenedithiol	0.2 A W ⁻¹	[263]
PbS + PCBM	Spin casting (100 nm thick)	Chlorobenzene	Oleic acid	0.32 A W ⁻¹	[265]
PbS + P3HT + PCBM	Doctor blading (100–250 nm thick)	Chlorobenzene	Oleic acid	51%	[267]

a)TOPO: trioctylphosphine oxide, TOP: trioctylphosphine, PMDTC: n-phenyl-N'-methyldithiocarbamate; b)EQE: external quantum efficiency.

a solution-processed CdSe-based transistor fabricated on a Kapton film. $^{[276]}$ Thiocyanate-exchanged CdSe NCs were spin-coated on an ultrathin Al_2O_3 dielectric layer, which effectively blocked the leakage currents (Figure 19b). They reported high-performance, low-hysteresis, and low-voltage CdSe NC transistors with electron mobilities up to 22 cm² V^{-1} s⁻¹ (Figure 19c). Moreover, aligned NWs have also been utilized in flexible transistors. $^{[277,278]}$ PbSe NWs capped with a hexadecane-*graft*-poly(vinylpyrrolidone) copolymer were drop-cast on an Al_2O_3 and octadecylphosphonic acid double dielectric layer and aligned across the device structure under an external electric field (Figure 19d). Figure 19e presents an SEM image

of the electrically aligned PbSe NWs. The i_D – V_G curves show reduced hysteresis and low-voltage transistor operation (Figure 19f). The detailed deposition conditions and device performances of key references are summarized in **Table 9**.

4.6. Memory Devices

NC-based memory devices have received great attention as next-generation non-volatile memory due to their scalability, small size, reliability, and high write/read/erase speeds.^[279,280] Various NCs of metals, semiconductors, and oxides have been

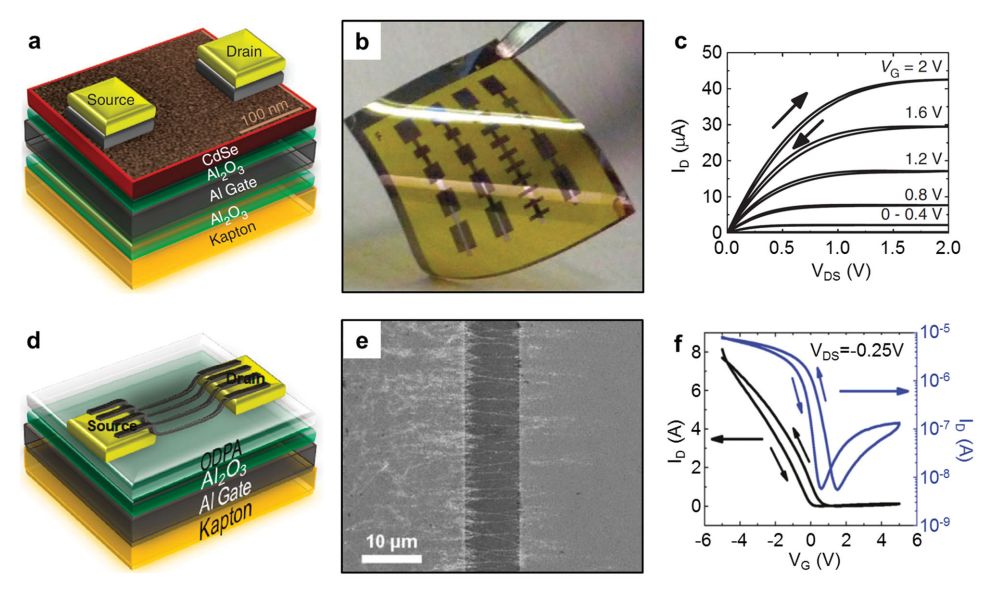


Figure 19. Transistors using NC layers. a) A schematic for the device structure of a flexible CdSe NC field-effect transistor. b) A photograph of a flexible CdSe NC field-effect transistor. c) Output drain current (I_D) versus drain-source voltage (V_{DS}) characteristics of the flexible CdSe NC field-effect transistor described in (a). d) A schematic of a flexible PbSe NW field-effect transistor. e) An SEM image of PbSe NWs aligned on a gold source—drain electrode. f) I_D – V_G characteristics showing the reduced hysteresis and low-voltage operation of the flexible PbSe NW field-effect transistor. a—c) Reproduced with permission. Copyright 2012, Nature Publishing Group. d,f) Reproduced with permission. Copyright 2011, American Chemical Society. e) Reproduced with permission. Royal Society of Chemistry.



ADVANCED MATERIALS

www.advmat.de

Table 9. Comparison of the transistor performance.

QD material	Printing method	Information of NC solution ^{a)}	Ligands	Mobility [cm 2 V $^{-1}$ s $^{-1}$]	Reference
CdSe	Drop casting	Pyridine	-	1	[269]
PbSe	Spin casting (900 rpm 10s $ ightarrow$ 1200 rpm 15s)	Octane (380 mg mL^{-1})	N ₂ H ₄ , CH ₃ NH ₂ , pyridine	-	[60]
	(50–450 nm thick)				
CdSe	Spin casting or drop casting	Hydrazine, water, DMSO, formamide, ethanolamine	$In_2Se_4^{\ 2^-},\ Sn_2S_6^{\ 4^-},\ In_2Te_3,\ Ga_2Se_3,\ CuInSe_2,\ ZnTe,\ HgSe_2^{\ 2^-},\ Sb_2Se_3$	0.03	[64]
		<10 wt%			
CdSe/ZnS, PbS	Dip coating	FA, DMSO, DMF, MeOH	SnS ₄ ⁴⁻ , Sn ₂ S ₆ ⁴⁻	-	[65]
CdSe	Spin casting (2000 rpm 30s)	Toluene (ca. 2 mg mL ⁻¹)	S ^{2–} , Se ^{2–} , Te ^{2–} , HS [–] , HSe [–] , HTe [–]	-	[262]
PbSe	Drop casting	Octane/nonane	-	-	[277]
CdSe	Spin casting (500 rpm 30s \rightarrow 800 rpm 30s)	DMF	Thiocyanate	22	[276]
CdSe	Spin casting (500 rpm 30s \rightarrow 800 rpm 30s)	DMF	Thiocyanate	-	[275]
PbSe	Drop casting	Chloroform/octane (1 µL)	-	-	[278]
PbS	Spin casting (4000 rpm)	(5 mg mL^{-1})	3-Mercaptopropionic acid, benzene- dithiol, ethandithiol	1.91 (e ⁻) 0.15 (h ⁺)	[272]
PbSe	Dip coating	Hexane (20 mg mL ⁻¹)	Alkanedithiol	_	[248]
CdSe	Spin casting (20–30 nm thick)	Hydrazine (15–30 mg mL ⁻¹)	In ₂ Se ₄ ²⁻	16	[273]
CdSe, InAs, PbTe	Spin casting (600rpm 6s \rightarrow 2000rpm 60s) (30–40 nm thick)	NMF (ca. 70 mg mL ⁻¹)	Cl ⁻ , l ⁻ , Br ⁻ , N ₃ ⁻ , I ₃ ⁻	12	[274]

^{a)}DMSO: dimethyl sulfoxide, DMF: dimethylformamide, NMF: N-methyl-formamide.

proposed as charge-trap sites in the floating gates of flash memories^[281] and as switchable resistive materials in resistive random-access memories.^[282,98] Here, we focus on NC-based flash memory.

Flash memory is a modified metal-oxide-semiconductor field-effect transistor (MOSFET) that has a floating gate (FG) inside the dielectric layer (Figure 20a, left). The data is stored/erased by injecting/removing carriers in the FG with a variation of the threshold voltage (Figure 20b). A thin tunneling oxide between the channels and the FG acts as a barrier to block undesirable charge leakage. With device scaling, the thickness of the tunneling oxide also decreases, which may lead to a large leakage current. To solve this issue, NC structures have been introduced in the FG. Previously, NCs were inserted in the FG layer using gas-phase deposition or thermal annealing of the thin film. However, it is difficult to control the charge-trap density and obtain a uniform distribution. Instead, colloidal NCs of semiconductors or metals are promising candidates for charge-trapping elements because monodisperse NCs can be closely packed at uniform distances (Figure 20a, right). Moreover, organic ligands on the surface of an NC can act as an additional charge barrier to prevent leakage currents. Si NCs (5 nm) were first introduced in the structure of flash memory by IBM in 1996, [283] and many NCs have been subsequently proposed. Among them, Au NCs were proposed as appropriate materials to serve as FGs due to their chemical stability, high work function, and deep quantum wall structure.

To fabricate high-performance memory devices, NCs can be carefully assembled by various processes. Spin casting is widely used to fabricate NC films (Figure 20c), but it is difficult to precisely control the NC thickness and orientation. Multilayered NCs enhance the charge capacity in the FGs, but a thicker film increases the threshold operating voltage. Caruso's group reported a charge-trap memory with layer-by-layer spin-coated NC layers and determined the thickness effects on the memory window and charge density.^[281] As the number of NC layer increases, the number density of the charge-storage elements (Au NCs) proportionally increases, while the electric field across the memory device decreases inversely. They showed that an optimal NC thickness could be achieved by a trilayer of NCs (Figure 20d). As a compact NC film is preferred to enhance the charge density of the flash memory, self-assembled NC layers have been intensively investigated. LB techniques are widely used to produce self-assembled high-density NC monolayers. [280] Roy and co-workers proposed flexible flash memories based on a high density Au NC monolayer fabricated by contact printing (Figure 20e). [284] The self-aligned NC monolayer was picked up with an elastomer stamp, dried, and released on the tunneling oxide layer.

5. Conclusion and Outlook

Colloidal synthesis approaches enable the delicate control of the size and shape of monodisperse NCs, which are key factors governing their properties and are not achievable using conventional routes including micro-fabrication processes. These free-standing materials can be deposited on virtually any kind of substrate through quite simple processes.



www.MaterialsViews

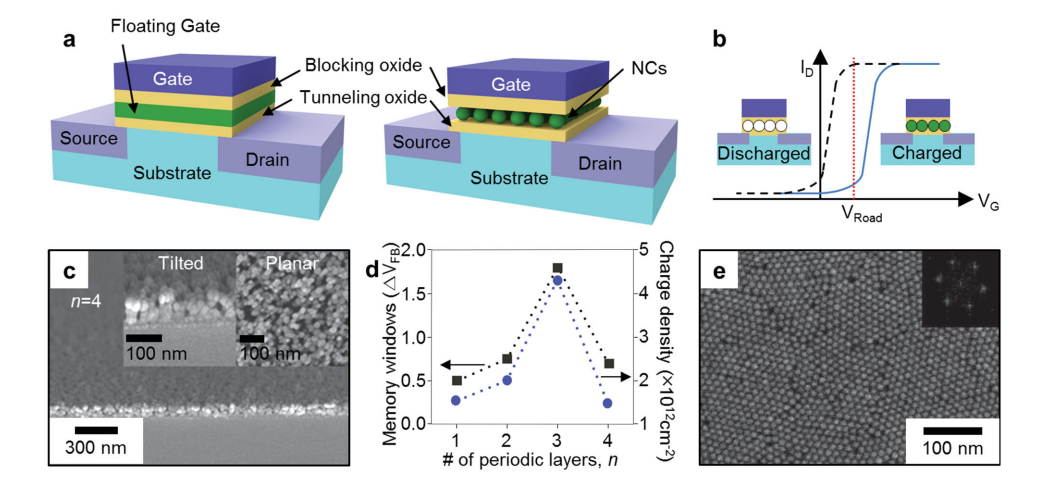


Figure 20. Memory devices using NC layers. a,b) Schematics of memory devices. c) Scanning electron microscopy images of the cross-section of a polyelectrolyte/AuNP triple-layer film obtained by the dip-coating process. The insets show the tilted (left side) and planar (right side) images magnified from the areas in the two red boxes. d) An atomic force microscopy image of the nanocomposite film containing NaYF4:Yb&Er/NaYF4 core/shell upconversion NCs and poly(3-hexylthiophene). e) An SEM image of the Au NP superlattice used in flexible flash memories. The superlattice was obtained by the microcontact printing. c,d) Reproduced with permission. [281] Copyright 2007, Nature Publishing Group. e) Reproduced with permission.[284]

These recent progresses in 2D/3D assembly methods, including film fabrication and printing methods, enable the designed integration of NC solids into various devices. Recently, the NC based electronic/optoelectronic devices have received tremendous attention from the industry because of the processability, deformability, and cost-effectiveness. For example, QLEDs take place as the next generation display and various NW based electrodes are being employed in flexible electronics.

There are still several issues, however, for successful commercialization of NC electronic/optoelectronic devices. In a long term view, devices employing environmentally benign and biocompatible NCs should replace electronics using NCs containing heavy metals. It is also important to develop advanced techniques for the integration and processing that control 2D/3D nanoarchitectures. For this issue, the use of NC superlattices is one of the important strategies. Fundamental understandings on the formation mechanism and collective properties resulting from NC superlattices will stimulate the fabrication of complex and sophisticated devices. The 2D/3D integration of NCs and their incorporation into devices on large scale are additional important challenges. Consequently, the development of new processes not only for novel and elaborate architectures but also for high reproducibility for large-scale production will shed light on the extensive commercialization of next-generation electronic and optoelectronic devices based on colloidal NCs.

Acknowledgements

J.Y. and M.K.C. contributed equally to this work. This work was supported by IBS-R006-D1.

> Received: June 13, 2015 Revised: July 31, 2015 Published online: December 28, 2015

- [1] A. L. Efros, M. Rosen, M. Kuno, M. Nirmal, D. J. Norris, M. Bawendi, Phys. Rev. B 1996, 54, 4843.
- [2] N. L. Rosi, C. A. Mirkin, Chem. Rev. 2005, 105, 1547.
- [3] D. J. Norris, A. L. Efros, S. C. Erwin, Science 2008, 319, 1776.
- [4] I. G. Mendintz, H. T. Uyeda, E. R. Goldman, H. Mattoussi, Nat. Mater. 2005, 4, 435.
- [5] A. J. Nozik, M. C. Beard, J. M. Luther, M. Law, R. J. Ellingson, J. C. Johnson, Chem. Rev. 2010, 110, 6873.
- [6] H. Goesmann, C. Feldmann, Angew. Chem. Int. Ed. 2010, 49,
- [7] B. Ji, E. Giovanelli, B. Habert, P. Spinicelli, M. Nasilowski, X. Xu, N. Lequeux, J.-P. Hugonin, F. Marquier, J.-J. Greffet, B. Dubertret, Nat. Nanotechnol. 2015. 10. 170.
- [8] D. J. Norris, Al. L. Efros, M. Rosen, M. G. Bawendi, Phys. Rev. B 1996, 53, 16347.
- [9] A. P. Alivisatos, Science 1996, 271, 933.
- [10] A.-H. Lu, E. L. Salabas, F. Schüth, Angew. Chem. Int. Ed. 2007, 46, 1222.
- [11] R. Hao, R. Xing, Z. Xu, Y. Hou, S. Gao, S. Sun, Adv. Mater. 2010, 22, 2729.
- [12] P. K. Jain, X. Huang, I. H. El-Sayed, M. A. El-Sayed, Plasmonics 2007. 2. 107.
- [13] S. Zeng, D. Baillargeat, H.-P. Ho, K.-T. Yong, Chem. Soc. Rev. 2014, 43, 3426.
- [14] J. H. Yu, X. Liu, K. E. Kweon, J. Joo, J. Park, K.-T. Ko, D. W. Lee, S. Shen, K. Tivakornsasithorn, J. S. Son, J.-H. Park, Y.-W. Kim, G. S. Hwang, M. Dobrowolska, J. K. Furdyna, T. Hyeon, Nat. Mater. 2010, 9, 47.
- [15] J. Yang, R. Fainblat, S. G. Kwon, F. Muckel, J. H. Yu, H. Terlinden, B. H. Kim, D. lavarone, M. K. Choi, I. Y. Kim, I. C. Park, H.-K. Hong, J. Lee, J. S. Son, Z. Lee, K. Kang, S.-J. Hwang, G. Bacher, T. Hyeon, J. Am. Chem. Soc. 2015, 137, 12776.
- [16] J. Park, J. Joo, S. G. Kwon, Y. Jang, T. Hyeon, Angew. Chem. Int. Ed. **2007**, 46, 4630.
- [17] J. Park, E. Kang, S. U. Son, H. M. Park, M. K. Lee, J. Kim, K. W. Kim, H. J. Noh, J. H. Park, C. J. Bae, J. G. Park, T. Hyeon, Adv. Mater. 2005, 17, 429.
- [18] S. Sun, C. B. Murray, D. Weller, L. Folks, A. Moser, Science 2000, 287, 1989.

ADVANCED MATERIALS

www.advmat.de

www.MaterialsViews.com

- [19] X. Lu, M. Rycenga, S. E. Skrabalak, B. Wiley, Y. Xia, Annu. Rev. Phys. Chem. 2009, 60, 167.
- [20] C. B. Murray, D. J. Norris, M. G. Bawendi, J. Am. Chem. Soc. 1993, 115, 8706.
- [21] W. W. Yu, X. Peng, Angew. Chem. Int. Ed. 2002, 41, 2368.
- [22] J. S. Son, K. Park, S. G. Kwon, J. Yang, M. Choi, J. Kim, J. H. Yu, J. Joo, T. Hyeon, Small 2012, 8, 2394.
- [23] Semiconductor Nanocrystal Quantum Dots: Synthesis, Assembly, Spectroscopy and Applications, (Ed: A. Rogach), Springer Verlag, Vienna. Austria. 2008.
- [24] J. S. Son, M. K. Choi, M.-K. Han, K. Park, J.-Y. Kim, S. J. Lim, M. Oh, Y. Kuk, C. Park, S.-J. Kim, T. Hyeon, *Nano Lett.* 2012, 12, 640.
- [25] T. Hyeon, S. S. Lee, J. Park, Y. Chung, H. B. Na, J. Am. Chem. Soc. 2001, 123, 12798.
- [26] J. Park, K. An, Y. Hwang, J.-G. Park, H.-J. Noh, J.-Y. Kim, J.-H. Park, N.-M. Hwang, T. Hyeon, *Nat. Mater.* 2004, 3, 891.
- [27] J. Joo, T. Yu, Y. W. Kim, H. M. Park, F. Wu, J. Z. Zhang, T. Hyeon, J. Am. Chem. Soc. 2003, 125, 6553.
- [28] C. Burda, X. Chen, R. Narayanan, M. A. El-Sayed, Chem. Rev. 2005, 105, 1025.
- [29] D. V. Talapin, J.-S. Lee, M. V. Kovalenko, E. V. Shevchenko, Chem. Rev. 2010, 110, 389.
- [30] K. Ariga, A. Vinu, Y. Yamauchi, Q. Ji, J. P. Hill, Bull. Chem. Soc. Jpn. 2012, 85, 1
- [31] J. Y. Kim, O. Voznyym, D. Zhitomirsky, E. H. Sargent, Adv. Mater. 2013, 25, 4986.
- [32] Y. Shirasaki, G. J. Supran, M. G. Bawendi, V. Bulovic, *Nat. Photonics* 2013, 7, 13.
- [33] J. Kim, M. Lee, H. J. Shim, R. Ghaffari, H. R. Cho, D. Son, Y. H. Jung, M. Soh, C. Choi, S. Jung, K. Chu, D. Jeon, S.-T. Lee, J. H. Kim, S. H. Choi, T. Hyeon, D.-H. Kim, *Nat. Commun.* 2014, 5. 5747.
- [34] M. K. Choi, O. K. Park, C. Choi, S. Qiao, R. Ghaffari, J. Kim, D. J. Lee, M. Kim, W. Hyun, S. J. Kim, H. J. Hwang, S.-H. Kwon, T. Hyeon, N. Lu, D.-H. Kim, Adv. Healthcare Mater. 2015, DOI: 10.1002/adhm.201500285.
- [35] M. V. Kovalenko, L. Manna, A. Cabot, Z. Hens, D. V. Talapin, C. R. Kagan, V. I. Klimov, A. L. Rogach, P. Reiss, D. J. Milliron, P. Guyot-Sionnnest, G. Konstantatos, W. J. Parak, T. Hyeon, B. A. Korgel, C. B. Murray, W. Heiss, ACS Nano 2015, 9, 1012.
- [36] A. Llordés, G. Garcia, J. Gazquez, D. J. Milliron, *Nature* 2013, 500, 323.
- [37] C. Kim, R. Buonsanti, R. Yaylian, D. J. Milliron, J. Cabana, Adv. Energy Mater. 2013, 3, 1286.
- [38] M. Murdoch, G. I. N. Waterhouse, M. A. Nadeem, J. B. Metson, M. A. Keane, R. F. Howe, J. Llorca, H. Idriss, Nat. Chem. 2011, 3, 489.
- [39] X. Chen, L. Liu, P. Y. Yu, S. S. Mao, Science 2011, 331, 746.
- [40] E. V. Shevchenko, D. V. Talapin, N. A. Kotov, S. O'Brien, C. B. Murray, *Nature* 2006, 439, 55.
- [41] M. K. Choi, J. Yang, K. Kang, D. C. Kim, C. Choi, C. Park, S. J. Kim, S. I. Chae, T.-H. Kim, J. H. Kim, T. Hyeon, D.-H. Kim, Nat. Commun. 2015, 6, 7149.
- [42] N. T. K. Thanh, N. Maclean, S. Mahiddine, Chem. Rev. 2014, 114, 7610.
- [43] S. G. Kwon, T. Hyeon, Acc. Chem. Res. 2008, 41, 1696.
- [44] C. R. Bullen, P. Mulvaney, Nano Lett. 2004, 4, 2303.
- [45] J. van Embden, P. Mulvaney, Langmuir 2005, 21, 10226.
- [46] Y. Yin, A. P. Alivisatos, Nature 2005, 437, 664.
- [47] Y. Xia, Y. Xiong, B. Lim, S. E. Skrabalak, Angew. Chem. Int. Ed. 2009, 48, 60.
- [48] J. Yang, J. S. Son, J. H. Yu, J. Joo, T. Hyeon, Chem. Mater. 2013, 25, 1190.
- [49] X. Peng, L. Manna, W. Yang, J. Wickham, E. Scher, A. Kadavanich, A. P. Alivisatos, *Nature* 2000, 404, 59.

- [50] L. Manna, D. J. Miliron, A. Meisel, E. C. Scher, A. P. Alivisatos, Nat. Mater. 2003, 2, 382.
- [51] J. Joo, J. S. Son, S. G. Kwon, J. H. Yu, T. Hyeon, J. Am. Chem. Soc. 2006, 128, 5632.
- [52] S. Ithurria, M. D. Tessier, B. Mahler, R. P. S. M. Lobo, B. Dubertret, A. L. Efros, *Nat. Mater.* **2011**, *10*, 936.
- [53] J. S. Son, X.-D. Wen, J. Joo, J. Chae, S.-i. Baek, K. Park, J. H. Kim, K. An, J. H. Yu, S. G. Kwon, S.-H. Choi, Z. Wang, Y.-W. Kim, Y. Kuk, R. Hoffmann, T. Hyeon, *Angew. Chem. Int. Ed.* **2009**, *48*, 6861.
- [54] A. Zabet-Khosousi, A. A. Dhirani, Chem. Rev. 2008, 108, 4072.
- [55] G. Konstantatos, I. Howard, A. Fischer, S. Hoogland, J. Clifford, E. Klem, L. Levina, E. H. Sargent, *Nature* 2006, 442, 180.
- [56] M. J. Hostetler, A. C. Templeton, R. W. Murray, *Langmuir* 1999, 15, 3782
- [57] N. Gaponik, D. V. Talapin, A. L. Rogach, A. Eychmuller, H. Weller, Nano Lett. 2002, 2, 803.
- [58] I. Lokteva, N. Radychev, F. Witt, H. Borchert, J. Parisi, J. Kolny-Olesiak, J. Phys. Chem. C 2010, 114, 12784.
- [59] D. W. Lucey, D. J. MacRae, M. Furis, Y. Sahoo, A. N. Cartwright, P. N. Prasad, Chem. Mater. 2005, 17, 3754.
- [60] D. V. Talapin, C. B. Murray, Science 2005, 310, 86.
- [61] M. Law, J. M. Luther, Q. Song, B. K. Hughes, C. L. Perkins, A. J. Nozik, J. Am. Chem. Soc. 2008, 130, 5974.
- [62] D. Yu, C. Wang, P. Guyot-Sionnest, Science 2003, 300, 1277.
- [63] K. Overgaag, P. Liljeroth, B. Grandidier, D. I. Vanmaekelbergh, ACS Nano 2008, 2, 600.
- [64] M. V. Kovalenko, M. Scheele, D. V. Talapin, Science 2009, 324, 1417.
- [65] M. V. Kovalenko, M. I. Bodnarchuk, J. Zaumseil, J.-S. Lee, D. V. Talapin, J. Am. Chem. Soc. 2010, 132, 10085.
- [66] A. T. Fafarman, W. K. Koh, B. T. Diroll, D. K. Kim, D. K. Ko, S. J. Oh, X. C. Ye, V. Doan-Nguyen, M. R. Crump, D. C. Reifsnyder, C. B. Murray, C. R. Kagan, J. Am. Chem. Soc. 2011, 133, 15753.
- [67] J. Huang, W. Liu, D. S. Dolzhnikov, L. Protesescu, M. V. Kovalenko, B. Koo, S. Chattopadhyay, E. V. Shevchenko, D. V. Talapin, ACS Nano 2014, 8, 9388.
- [68] D. N. Dirin, S. Dreyfuss, M. I. Bodnarchuk, G. Nedelcu, P. Papagiorgis, G. Itskos, M. V. Kovalenko, J. Am. Chem. Soc. 2014, 136, 6550.
- [69] A. Nag, H. Zhang, E. Janke, D. V. Talapin. Z. Phys. Chem. 2014, 229, 85.
- [70] T.-H. Kim, D.-Y. Chung, J. Ku, I. Song, S. Sul, D.-H. Kim, K.-S. Cho, B. L. Choi, J. M. Kim, S. Hwang, K. Kim, *Nat. Commun.* 2013, 4, 2637.
- [71] C. B. Murray, C. R. Kagan, M. G. Bawendi, Science 1995, 270, 1335.
- [72] C. B. Murray, C. R. Kagan, M. G. Bawendi, Annu. Rev. Mater. Sci. 2000, 30, 545.
- [73] S. Coe, W.-K. Woo, M. G. Bawendi, V. Bulović, Nature 2002, 420, 800.
- [74] L. Etgar, D. Yanover, R. K. apek, R. Vaxenburg, Z. Xue, B. Liu, M. K. Nazeeruddin, E. Lifshitz, M. Grätzel, Adv. Funct. Mater. 2012, 23, 2736.
- [75] I. Gur, N. A. Fromer, M. L. Geier, A. P. Alivisatos, *Science* 2005, 310, 462.
- [76] M. Park, K. Do, J. Kim, D. Son, J. H. Koo, J. Park, J.-K. Song, J. H. Kim, M. Lee, T. Hyeon, D.-H. Kim, Adv. Healthcare Mater. 2015, 4, 992.
- [77] C. J. Lawrence, Phys. Fluids 1988, 31, 2786.
- [78] K. Norrman, A. G. -Siahkali, N. B. Larsen, Annu. Rep. Prog. Chem., Sect. C 2005, 101, 174.
- [79] L. L. Spangler, J. M. Torkelson, J. S. Royal, Polym. Eng. Sci. 1990, 30, 644.
- [80] J. M. Luther, M. Law, Q. Song, C. L. Perkins, M. C. Beard, A. J. Nozik, ACS Nano 2008, 2, 271.
- [81] E. Talgorn, Y. Gao, M. Aerts, L. T. Kunneman, J. M. Schins, T. J. Savenije, M. A. van Huis, H. S. J. van der Zant, A. J. Houtepen, L. D. A. Siebbeles, *Nat. Nanotechnol.* 2011, 6, 733.



vana Materials Views com

- [82] Y. Gao, M. Aerts, C. S. S. Sandeep, E. Talgorn, T. J. Savenije, S. Kinge, L. D. A. Siebbeles, A. J. Houtepen, ACS Nano 2012, 6, 9606.
- [83] D. Son, J. Lee, D. J. Lee, R. Ghaffari, S. Yun, S. J. Kim, J. E. Lee, H. R. Cho, S. Yoon, S. Yang, S. Lee, S. Qiao, D. Ling, S. Shin, J.-K. Song, J. Kim, T. Kim, H. Lee, J. Kim, M. Soh, N. Lee, C. S. Hwang, S. Nam, N. Lu, T. Hyeon, S. H. Choi, D.-H. Kim, ACS Nano 2015, 9, 5937.
- [84] L. D. Landau, V. G. Levich, Acta Physicochim. URSS 1942, 17, 42.
- [85] E. A. Gaulding, B. T. Dirool, E. D. Goodwin, Z. J. Vrtis, C. R. Kagan, C. B. Murray, Adv. Mater. 2015, 27, 2846.
- [86] L.E. Scriven, C. V. Stcrnling, Nature 1960, 187, 186.
- [87] H. Dislieh, P. Hinz, J. Non-Cryst. Solids 1982, 48, 11.
- [88] K. B. Blodgett, J. Am. Chem. Soc. 1934, 56, 495.
- [89] B. O. Dabbousi, C. B. Murray, M. F. Rubner, M. G. Bawendi, *Chem. Mater.* 1994, 6, 216.
- [90] T. Fried, G. Shemer, G. Markovich, Adv. Mater. 2001, 13, 1158.
- [91] C. P. Collier, R. J. Saykally, J. J. Shiang, S. E. Henrichs, J. R. Heath, Science 1997, 277, 1978.
- [92] D.-M. Smilgies, A. T. Heitsch, B. A. Korgel, J. Phys. Chem. B 2012, 116, 6017.
- [93] H. Song, F. Kim, S. Connor, G. A. Somorjai, P. Yang, J. Phys. Chem. B 2005, 109, 188.
- [94] F. Kim, S. Kwan, J. Akana, P. Yang, J. Am. Chem. Soc. 2001, 123,
- [95] A. Tao, F. Kim, C. Hess, J. Goldberger, R. He, Y. Sun, Y. Xia, P. Yang, Nano Lett. 2003, 3, 1229.
- [96] S. Acharya, A. B. Panda, N. Belman, S. Efrima, Y. Golan, Adv. Mater. 2006, 18, 210.
- [97] K. Lambert, Y. Justo, J. S. Kamal, Z. Hens, Angew. Chem. Int. Ed. 2011, 50, 12058.
- [98] D. Son, J. Lee, S. Qiao, R. Ghaffari, J. Kim, J. E. Lee, C. Song, S. J. Kim, D. J. Lee, S. W. Jun, S. Yang, M. Park, J. Shin, K. Do, M. Lee, K. Kang, C. S. Hwang, N. Lu, T. Hyeon, D.-H. Kim, Nat. Nanotechnol. 2014, 9, 397.
- [99] S. Srivastava, D. Nykypanchuk, M. Fukuto, O. Gang, ACS Nano 2014, 8, 9857.
- [100] W. Wang, X. Chen, S. Efrima, Chem. Mater. 1999, 11, 1883.
- [101] A. R. Tao, J. Huang, P. Yang, Acc. Chem. Res. 2008, 41, 1662.
- [102] S. Acharya, J. P. Hill, K. Ariga, Adv. Mater. 2009, 21, 2959.
- [103] F. C. Krebs, Sol. Energy Mater. Sol. Cells 2009, 93, 394.
- [104] C.-Y. Cai, K.-Y. A. Lin, H. Yang, Appl. Phys. Lett. 2014, 105, 201913.
- [105] J. Krantz, M. Richter, S. Spallek, E. Spiecker, C. J. Brabec, Adv. Funct. Mater. 2011, 21, 4784.
- [106] M. K. Nazeeruddin, F. De Angelis, S. Fantacci, A. Selloni, G. Viscardi, P. Liska, S. Ito, T. Bessho, M. Grätzel, J. Am. Chem. Soc. 2005, 127, 16835.
- [107] H. Choi, S. Kim, S. O. Kang, J. Ko, M.-S. Kang, J. N. Clifford, A. Forneli, E. Palomares, M. K. Nazeeruddin, M. Grätzel, Angew. Chem. Int. Ed. 2008, 47, 8259.
- [108] J. Yang, J.-Y. Kim, J. H. Yu, T.-Y. Ahn, H. Lee, T.-S. Choi, Y.-W. Kim, J. Joo, M. J. Ko, T. Hyeon, *Phys. Chem. Chem. Phys.* 2013, 15, 20517.
- [109] B. J. Alder, W. G. Hoover, D. A. Young, J. Chem. Phys. 1968, 49, 3688.
- [110] P. G. Bolhuis, D. Frenkel, S.-C. Mau, D. A. Huse, *Nature* 1997, 388, 235.
- [111] D. V. Talapin, E. V. Shevchenko, C. B. Murray, A. V. Titov, P. Kral, Nano Lett. 2007, 7, 1213.
- [112] D. V. Talapin, E. V. Shevchenko, C. B. Murray, A. Kornowski, S. Förster, H. Weller, J. Am. Chem. Soc. 2004, 126, 12984.
- [113] B. T. Diroll, N. J. Greybush, C. R. Kagan, C. B. Murray, Chem. Mater. 2015, 27, 2998.
- [114] Z. Chen, J. Moore, G. Radtke, H. Sirringhaus, S. O'Brien, J. Am. Ch em. Soc. 2007, 129, 15702.

- [115] F. X. Redl, K. S. Cho, C. B. Murray, S. O'Brien, Nature 2003, 423, 968.
- [116] B. A. Boles, D. V. Talapin, J. Am. Chem. Soc. 2015, 137, 4494.
- [117] Y. Min, M. Akbulut, K. Kristiansen, Y. Golan, J. Israelachvili, Nat. Mater. 2008, 7, 527.
- [118] L.-S. Li, A. P. Alivisatos, Phys. Rev. Lett. 2003, 90, 097402.
- [119] M. Shim, P. Guyot-Sionnest, J. Phys. Chem. 1999, 111, 6955.
- [120] M. A. Islam, Y. Xia, M. L. Steigerwald, M. Yin, Z. Liu, S. O'Brien, R. Levicky, I. P. Herman, *Nano Lett.* 2003, 3, 1603.
- [121] B. A. Korgel, S. Fullam, S. Connolly, D. Fitzmaurice, J. Phys. Chem. B 1998, 102, 8379.
- [122] K. S. Martirosyan, C. Dannangoda, E. Galstyan, D. Litvinov, J. Appl. Phys. 2012, 111, 094311.
- [123] A. A. Bessonov, M. N. Kirikova, D. I. Petukhov, M. Allen, T. Ryhänen, M. J. A. Bailey, *Nat. Mater.* **2015**, *14*, 199.
- [124] L. Liu, X. Wan, L. Sun, S. Yang, Z. Dai, Q. Tian, M. Lei, X. Xiao, C. Jiang, W. Wu, RSC Adv. 2015, 5, 9783.
- [125] S. Ito, P. Chen, P. Comte, M. K. Nazeeruddin, P. Liska, P. Péchy, M. Grätzel, Prog. Photovoltaics: Res. Appl. 2007, 15, 603.
- [126] T. H. J. van Osch, J. Perelaer, A. W. M. de Laat, U. S. Schubert, Adv. Mater. 2008, 20, 343.
- [127] J. Bharathan, Y. Yang, Appl. Phys. Lett. 1998, 72, 2660.
- [128] B. S.-C. Chang, J. Liu, J. Bharathan, Y. Yang, J. Onohara, J. Kido, Adv. Mater. 1999, 11, 734.
- [129] R. F. Service, Science 2004, 304, 675.
- [130] J.-S. Yu, I. Kim, J.-S. Kim, J. Jo, T. T. Larsen-Olsen, R. R. Søndergaard, M. Hösel, D. Angmo, M. Jørgensen, F. C. Krebs, *Nanoscale* 2012, 4, 6032.
- [131] Y. Oh, J. Kim, Y. J. Yoon, H. Kim, H. G. Yoon, S.-N. Lee, J. Kim, Curr. Appl. Phys. 2011, 11, S359.
- [132] K. J. Lee, B. H. Jun, T. H. Kim, J. Joung, Nanotechnology 2006, 17, 2424.
- [133] R. D. Deegan, O. Bakajin, T. F. Dupont, G. Huber, S. R. Nagel, T. A. Witten, *Nature* **1997**, *389*, 827..
- [134] D. Pesach, A. Marmur, Langmuir 1987, 3, 519.
- [135] R. D. Deegan, O. Bakajin, T. F. Dupont, G. Huber, S. R. Nagel, T. A. Witten, *Phys. Rev. E* **2000**, *62*, 756.
- [136] K. Fukuda, T. Sekine, D. Kumaki, S. Tokito, ACS Appl. Mater. Interfaces 2013, 5, 3916.
- [137] B.-J. de Gans, U. S. Schubert, Langmuir 2004, 20, 7789.
- [138] E. Tekin, P. J. Smith, S. Hoeppener, A. M. J. van den Berg, A. S. Susha, A. L. Rogach, J. Feldmann, U. S. Schubert, Adv. Funct. Mater. 2007, 17, 23.
- [139] H. Hu, R. G. Larson, Langmuir 2005, 21, 3972.
- [140] V. Wood, M. J. Panzer, J. Chen, M. S. Bradley, J. E. Halpert, M. G. Bawendi, V. Bulović, Adv. Mater. 2009, 21, 2151.
- [141] B. H. Kim, M. S. Onses, J. B. Lim, S. Nam, N. Oh, H. Kim, K. J. Yu, J. W. Lee, J.-H. Kim, S.-K. Kang, C. H. Lee, J. Lee, J. H. Shin, N. H. Kim, C. Leal, M. Shim, J. A. Rogers, *Nano Lett.* 2015, 15, 969.
- [142] B. Y. Ahn, E. B. Duoss, M. J. Motala, X. Guo, S.-I. Park, Y. Xiong, J. Yoon, R. G. Nuzzo, J. A. Rogers, J. A. Lewis, *Science* 2009, 323, 1591.
- [143] J. T. Muth, D. M. Vogt, R. L. Truby, Y. Mengüç, D. B. Kolesky, R. J. Wood, J. A. Lewis, Adv. Mater. 2014, 26, 6307.
- [144] J. J. Adams, E. B. Duoss, T. F. Malkowski, M. J. Motala, B. Y. Ahn, R. G. Nuzzo, J. T. Bernhard, J. A. Lewis, Adv. Mater. 2011, 23, 1335.
- [145] B. Y. Ahn, E. B. Duoss, M. J. Motala, X. Guo, S.-I. Park, Y. Xiong, J. Yoon, R. G. Nuzzo, J. A. Rogers, J. A. Lewis, *Science* 2009, 323, 1590.
- [146] V. Reboud, N. Kehagias, M. Zelsmann, M. Striccoli, M. Tamborra, M. L. Curri, A. Agostiano, D. Mecerreyes, J. A. Alduncín, C. M. S. Torres, *Microeletron. Eng.* 2007, 84, 1574.
- [147] M. Tamborra, M. Striccoli, M. L. Curri, J. A. Alducin, D. Mecerreyes, J. A. Pomposo, N. Kehagias, V. Reboud, C. M. S. Torres, A. Agostiano, Small 2007, 3, 822.

www.MaterialsViews.com

- [148] A. T. Fafarman, S.-H. Hong, H. Caglayan, X. Ye, B. T. Diroll, T. Paik, N. Engheta, C. B. Murray, C. R. Kagan, Nano Lett. 2013, 13, 350.
- [149] V. Reboud, N. Kehagias, C. M. S. Torres, M. Zelsmann, M. Striccoli, M. L. Curri, A. Agostiano, M. Tamborra, M. Fink, F. Reuther, G. Gruetzner, Appl. Phys. Lett. 2007, 90, 011115.
- [150] V. Reboud, N. Kehagias, M. Zelsmann, M. Striccoli, M. Tamborra, M. L. Curri, A. Agostiano, M. Fink, F. Reuther, G. Gruetzner, C. M. S. Torres, J. Nanosci. Nanotechnol. 2008, 8, 535.
- [151] S. Zankovych, T. Hoffmann, J. Seekamp, J.-U. Bruch, C. M. Sotomayor-Torres, Nanotechnology 2001, 12, 91.
- [152] L. J. Guo, Adv. Mater. 2007, 19, 495.
- [153] A. Carlson, A. M. Bowen, Y. Huang, R. G. Nuzzo, J. A. Rogers, Adv. Mater. 2012, 24, 5284.
- [154] S. H. Sung, H. Yoon, J. Lim, K. Char, Small 2012, 8, 826.
- [155] T. Kraus, L. Malaquin, H. Schmid, W. Riess, N. D. Spencer, H. Wolf, Nat. Nanotechnol. 2007, 2, 570.
- [156] A. Gopal, K. Hoshino, S. Kim, X. Zhang, Nanotechnology 2009, 20, 235201.
- [157] L. Kim, P. O. Anikeeva, S. A. Coe-Sullivan, J. S. Steckel, M. G. Bawendi, V. Bulović, Nano Lett. 2008, 8, 4513.
- [158] A. Rizzo, M. Mazzeo, M. Biasiucci, R. Cingolani, G. Gigli, Small 2008, 4, 2143.
- [159] M. Xue, Z. Zhang, N. Zhu, F. Wang, X. Zhao, T. Cao, Langmuir 2009. 25. 4347.
- [160] T.-H. Kim, K.-S. Cho, E. K. Lee, S. J. Lee, J. Chae, J. W. Kim, D. H. Kim, J.-Y. Kwon, G. Amaratunga, S. Y. Lee, B. L. Choi, Y. Kuk, J. M. Kim, K. Kim, Nat. Photonics 2011, 5, 176.
- [161] M. C. McAlpine, H. Ahmad, D. Wang, J. R. Heath, Nat. Mater. **2007**, *6*, 379.
- [162] J. A. Lewis, Adv. Funct. Mater. 2006, 16, 2193.
- [163] N. C. Schirmer, S. Ströhle, M. K. Tiwari, D. Poulikakos, Adv. Funct. Mater. 2011, 21, 388.
- [164] D. Lin, Q. Nian, B. Deng, S. Jin, Y. Hu, W. Wang, G. J. Cheng, ACS Nano 2014, 8, 9710.
- [165] L. C. Montemayor, L. R. Meza, J. R. Greer, Adv. Eng. Mater. 2014, 16, 184.
- [166] D. Jang, L. R. Meza, F. Greer, J. R. Greer, Nat. Mater. 2013, 12, 893.
- [167] K. Sun, T.-S. Wei, B. Y. Ahn, J. Y. Seo, S. J. Dillon, J. A. Lewis, Adv. Mater. 2013, 25, 4539.
- [168] C. Kullmann, N. C. Schirmer, M.-T. Lee, S. H. Ko, N. Hotz, C. P. Grigoropoulos, D. Poulikakos, J. Micromech. Microeng. 2012, 22, 055022.
- [169] Y. L. Kong, I. A. Tamargo, H. Kim, B. N. Johnson, M. K. Gupta, T.-W. Koh, H.-A. Chin, D. A. Steingart, B. P. Rand, M. C. McAlpine, Nano Lett. 2014, 14, 7017.
- [170] K. Kim, W. Zhu, X. Qu, C. Aaronson, W. R. McCall, S. Chen, D. J. Sirbuly, ACS Nano 2014, 8, 9799.
- [171] Y. Kashiwagi, A. Koizumi, Y. Takemura, S. Furuta, M. Yamamoto, M. Saitoh, M. Takahashi, T. Ohno, Y. Fujiwara, K. Murahashi, K. Ohtsuka, M. Nakamoto, Appl. Phys. Lett. 2014, 105, 223509.
- [172] H. Wu, L. B. Hu, M. W. Rowell, D. S. Kong, J. J. Cha, J. R. McDonough, J. Zhu, Y. A. Yang, M. D. McGehee, Y. Cui, Nano Lett. 2010, 10, 4242.
- [173] A. R. Rathmell, S. M. Bergin, Y. L. Hua, Z. Y. Li, B. J. Wiley, Adv. Mater. 2010, 22, 3558.
- [174] J.-Y. Lee, S. T. Connor, Y. Cui, P. Peumans, Nano Lett. 2008, 8,
- [175] J. Krantz, T. Stubhan, M. Richter, S. Spallek, I. Litzov, G. J. Matt, E. Spiecker, C. J. Brabec, Adv. Funct. Mater. 2013, 23, 1711.
- [176] A. R. Madaria, A. Kumar, F. N. Ishikawa, C. Zhou, Nano Res. 2010, 3. 564.
- [177] P. Lee, J. Lee, H. Lee, J. Yeo, S. Hong, K. H. Nam, D. Lee, S. S. Lee, S. H. Ko, Adv. Mater. 2012, 24, 3326.
- [178] L. Hu, H. S. Kim, J.-Y. Lee, P. Peumans, Y. Cui, ACS Nano 2010, 4, 2955.

- [179] M.-S. Lee, K. Lee, S.-Y. Kim, H. Lee, J. Park, K.-H. Choi, H.-K. Kim, D.-G. Kim, D.-Y. Lee, S.W. Nam, J.-U. Park, Nano Lett. 2013, 13, 2814.
- [180] J. Ge, H.-B. Yao, X. Wang, Y.-D. Ye, J.-L. Wang, Z.-Y. Wu, J.-W. Liu, F.-J. Fan, H.-L. Gao, C.-L. Zhang, S.-H. Yu, Angew. Chem. Int. Ed. **2013**, 52, 1654.
- [181] C. Yan, W. Kang, J. Wang, M. Cui, X. Wang, C. Y. Foo, K. J. Chee, P. S. Lee, ACS Nano 2014, 8, 316.
- [182] S. Choi, J. Park, W. Hyun, J. Kim, J. Kim, Y. B. Lee, C. Song, H. J. Hwang, J. H. Kim, T. Hyeon, D.-H. Kim, ACS Nano 2015, 9, 6626.
- [183] C. Jeong, P. Nair, M. Khan, M. Lundstrom, M. A. Alam, Nano Lett. 2011, 11, 5020.
- [184] I. N. Kholmanov, M. D. Stoller, J. Edgeworth, W. H. Lee, H. Li, J. Lee, C. Barnhart, J. R. Potts, R. Piner, D. Akinwande, J. E. Barrick, R. S. Ruoff, ACS Nano 2012, 6, 5157.
- [185] I. N. Kholmanov, C. W. Magnuson, A. E. Aliev, H. Li, B. Zhang, J. W. Suk, L. L. Zhang, E. Peng, S. H. Mousavi, A. B. Khanikaev, R. Piner, G. Shvets, R. S. Ruoff, Nano Lett. 2012, 12, 5679.
- [186] S. Lim, D. Son, J. Kim, Y. B. Lee, J.-K. Song, S. Choi, D. J. Lee, J. H. Kim, M. Lee, T. Hyeon, D.-H. Kim, Adv. Funct. Mater. 2015,
- [187] H. Lee, K. Lee, J. T. Park, W. C. Kim, H. Lee, Adv. Funct. Mater. 2014, 24, 3276.
- [188] I. K. Moon, J. I. Kim, H. Lee, K. Hur, W. C. Kim, H. Lee, Sci. Rep. 2013, 3, 1112.
- [189] W. Gaynor, G. F. Burkhard, M. D. McGehee, P. Peumans, Adv. Mater. 2011, 23, 2905.
- [190] R. Zhu, C.-H. Chung, K. C. Cha, W. Yang, Y. B. Zheng, H. Zhou, T.-B. Song, C.-C. Chen, P. S. Weiss, G. Li, Y. Yang, ACS Nano 2011, 5. 9877.
- [191] J. Lee, I. Lee, T.-S. Kim, J.-Y. Lee, Small 2013, 9, 2887.
- [192] X.-Y. Zeng, Q.-K. Zhang, R.-M. Yu, C.-Z. Lu, Adv. Mater. 2010, 22, 4484.
- [193] L. Li, Z. Yu, W. Hu, C.-H. Chang, Q. Chen, Q. Pei, Adv. Mater. 2011, 23, 5563.
- [194] Z. Yu, Q. Zhang, L. Li, Q. Chen, X. Niu, J. Liu, Q. Pei, Adv. Mater. 2011, 23, 664.
- [195] J. Liang, L. Li, X. Niu, Z. Yu, Q. Pei, Nat. Photonics 2013, 7, 817.
- [196] P.-C. Hsu, X. Liu, C. Liu, X. Xie, H. R. Lee, A. J. Welch, T. Zhao, Y. Cui, Nano Lett. 2015, 15, 365.
- [197] F. Xu, Y. Zhu, Adv. Mater. 2012, 24, 5117.
- [198] J. Ziegler, S. Xu, E. Kucur, F. Meister, M. Batentschuk, F. Gindele, T. Nann, Adv. Mater. 2008, 20, 4068.
- [199] M. J. Bowers, J. R. McBride, S. J. Rosenthal, J. Am. Chem. Soc. **2005**, *127*, 15378.
- [200] Q. Zhang, T. Xu, D. Butterfield, M. J. Misner, D. Y. Ryu, T. Emrick, T. P. Russell, Nano Lett. 2005, 5, 357.
- [201] H. S. Chen, S. J. J. Wang, C. J. Lo, J. Y. Chi, Appl. Phys. Lett. 2005, 86, 131905.
- [202] M. Achermann, M. A. Petruska, D. D. Koleske, M. H. Crawford, V. I. Klimov, Nano Lett. 2006, 6, 1396.
- [203] E. Jang, S. Jun, H. Jang, J. Lim, B. Kim, Y. Kim, Adv. Mater. 2010, 22, 3076.
- [204] X. Dai, Z. Zhang, Y. Jin, Y. Niu, H. Cao, X. Liang, L. Chen, J. Wang, X. Peng, Nature 2014, 515, 96.
- [205] J. M. Caruge, J. E. Halpert, V. Wood, V. Bulovic, M. G. Bawendi, Nat. Photonics 2008, 2, 247.
- [206] Q. Sun, Y. A. Wang, L. S. Li, D. Wang, T. Zhu, J. Xu, C. Yang, Y. Li, Nat. Photonics **2007**, 1, 717.
- [207] M. K. Choi, I. Park, D. C. Kim, E. Joh, O. K. Park, J. Kim, M. Kim, C. Choi, J. Yang, K. W. Cho, J.-H. Hwang, J.-M. Nam, T. Hyeon, J. H. Kim, D.-H. Kim, Adv. Funct. Mater. 2015, DOI: 10.1002/ adfm.201502956.
- [208] P. O. Anikeeva, J. E. Halpert, M. G. Bawendi, V. Bulović, Nano Lett. **2009**, 9, 2532.



354.



- [236] K. S. Leschkies, A. G. Jacobs, D J. Norries, E. S. Aydil, Appl. Phys.
- [210] K.-S. Cho, E. K. Lee, W.-J. Joo, E. Jang, T.-H. Kim, S. J. Lee, S.-J. Kwon, J. Y. Han, B.-K. Kim, B. L. Choi, J. M. Kim, Nature Photonics 2009, 3, 341.

[209] V. L. Colvin, M. C. Schlamp, A. P. Alivisatos, Nature 1994, 370,

- [211] W. K. Bae, J. Lim, D. Lee, M. Park, H. Lee, J. Kwak, K. Char, C. Lee, S. Lee, Adv. Mater. 2014, 26, 6387.
- [212] J. Kwak, W. K. Bae, D. Lee, I. Park, J. Lim, M. Park, H. Cho, H. Woo, D. Y. Yoon, K. Char, S. Lee, C. Lee, Nano Lett. 2012, 12, 2362.
- [213] J. Lim, W. K. Bae, D. Lee, M. K. Nam, J. Jung, C. Lee, K. Char, S. Lee, Chem. Mater. 2011, 23, 4459.
- [214] J. Lim, M. Park, W. K. Bae, D. Lee, S. Lee, C. Lee, K. Char, ACS Nano 2013, 7, 9019.
- [215] W. K. Bae, Y.-S. Park, J. Lim, D. Lee, L. A. Padilha, H. McDaniel, I. Robel, C. Lee, J. M. Pietryga, V. I. Klimov, Nat. Commun. 2013,
- [216] Y. Yang, Y. Zheng, W. Cao, A. Titov, J. Hyvonen, J. R. Manders, J. Xue, P. H. Holloway, L. Qian, Nat. Photonics 2015, 9, 259.
- [217] W. K. Bae, J. Kwak, J. Lim, D. Lee, M. K. Nam, K. Char, C. Lee, S. Lee, Nano Lett. 2010, 10, 2368.
- [218] B. S. Mashford, M. Stevenson, Z. Popovic, C. Hamilton, Z. Zhou, C. Breen, J. Steckel, V. Bulović, M. Bawendi, S. Coe-Sullivan, P. T. Kazlas, Nat. Photonics 2013, 7, 407.
- [219] L. Qian, Y. Zheng, J. Xue, P. H. Holloway, Nat. Photonics 2011, 5. 543.
- [220] J. S. Steckel, P. Snee, S. Coe-Sullivan, J. P. Zimmer, J. E. Halpert, P. Anikeeva, L.-A. Kim, V. Bulović, M. G. Bawendi, Angew. Chem. Int. Ed. 2006, 45, 5796.
- [221] Y. Zhang, C. Xie, H. Su, J. Liu, S. Pickering, Y. Wang, W. W. Yu, J. Wang, Y. Wang, J.-i. Hahm, N. Dellas, S. E. Mohney, J. Xu, Nano Lett. 2011, 11, 329.
- [222] P. O. Anikeeva, J. E. Halpert, M. G. Bawendi, V. Bulović, Nano Lett. **2007**. 7. 2196.
- [223] C. R. Kagan, C. B. Murray, M. Nirmal, M. G. Bawendi, Phys. Rev. Lett. 1996, 76, 3043.
- [224] S. A. McDonald, G. Konstantatos, S. Zhang, P. W. Cyr, E. J. D. Klem, L. Levina, E. H. Sargent, Nat. Mater. 2005, 4, 138.
- [225] A. H. Ip, S. M. Thon, S. Hoogland, O. Voznyy, D. Zhitomirsky, R. Debnath, L. Levina, L. R. Rollny, G. H. Carey, A. Fischer, K. W. Kemp, I. J. Kramer, Z. Ning, A. J. Labelle, K. W. Chou, A. Amassian, E. H. Sargent, Nat. Nanotechnol. 2012, 7, 577.
- [226] C.-H. M. Chuang, P. R. Brown, V. Bulović, M. G. Bawendi, Nat. Mater. 2014, 13, 796.
- [227] A. Zaban, O. I. Mićić, B. A. Gregg, A. J. Nozik, Langmuir 1998, 14, 3153.
- [228] B.-R. Hyun, Y.-W. Zhong, A. C. Bartnik, L. Sun, H. D. Abruña, F. W. Wise, J. D. Goodreau, J. R. Matthews, T. M. Leslie, N. F. Borrelli, ACS Nano 2008, 2, 2206.
- [229] H. Lee, M. Wang, P. Chen, D. R. Gamelin, S. M. Zakeeruddin, M. Grätzel, M. K. Nazeeruddin, Nano Lett. 2009, 9, 4221.
- [230] K. Zhao, Z. Pan, I. Mora-Seró, E. Cánovas, H. Wang, Y. Song, X. Gong, J. Wang, M. Bonn, J. Bisquert, X. Zhong, J. Am. Chem. Soc. 2015, 137, 5602.
- [231] G. I. Koleilat, L. Levina, H. Shukla, S. H. Myrskog, S. Hinds, A. G. Pattantyus-Abraham, E. H. Sargent, ACS Nano 2008, 2, 833.
- [232] J. M. Luther, M. Law, M. C. Beard, Q. Song, M. O. Reese, R. J. Ellingson, A. J. Nozik, Nano Lett. 2008, 8, 3488.
- [233] E. J. D. Klem, D. D. MacNeil, L. Levina, E. H. Sargent, Adv. Mater. **2008**, 20, 3433.
- [234] M. Law, M. C. Beard, S. Choi, J. M. Luther, M. C. Hanna, A. J. Nozik, Nano Lett. 2008, 8, 3904.
- [235] A. G. Pattantyus-Abraham, I. J. Kramer, A. R. Barkhouse, X. Wang, G. Konstantatos, R. Debnath, L. Levina, I. Raabe, M. K. Nazeeruddin, M. Grätzel, E. H. Sargent, ACS Nano 2010, 4, 3374.

- Lett. 2009, 93, 193103. [237] X. Wang, G. I. Koleilat, J. Tang, H. Liu, I. J. Kramer, R. Debnath,
- L. Brzozowski, D. A. R. Barkhouse, L. Levina, S. Hoogland, E. H. Sargent, Nat. Photonics 2011, 5, 480.
- [238] S. J. Kim, W. J. Kim, A. N. Cartwright, P. N. Prasad, Appl. Phys. Lett. 2008, 92, 191107.
- [239] B. Q. Sun, E. Marx, N. C. Greenham, Nano Lett. 2003, 3, 961.
- [240] S. Gunes, H. Neugebauer, N. S. Sariciftci, H. Roither, M. Kovalenko, G. Pillwein, W. Heiss, Adv. Funct. Mater. 2006, 16, 1095.
- [241] I. Gur, N. A. Fromer, C.-P. Chen, A. G. Kanaras, A. P. Alivisatos, Nano Lett. 2007, 7, 409.
- [242] K. P. Fritz, S. Guenes, J. Luther, S. Kumar, N. S. Saricifitci, G. D. Scholes, J. Photochem. Photobiol., A: Chem. 2008, 195, 39.
- [243] D. A. R. Barkhouse, R. Debnath, I. J. Kramer, D. Zhitomirsky, A. G. Pattantyus-Abraham, L. Levina, L. Etgar, M. Grätzel, E. H. Sargent, Adv. Mater. 2011, 23, 3134.
- [244] J. Lim, D. Lee, M. Park, J. Song, S. Lee, M. S. Kang, C. Lee, K. Char, J. Phys. Chem. C. 2014, 118, 3942.
- [245] J.-Y. Kim, J. Yang, J. H. Yu, W. Baek, C.-H. Lee, H. J. Son, T. Hyeon, M. J. Ko, ACS Nano 2015, DOI: 10.1021/acsnano.5b04917.
- [246] M. C. Beard, A. G. Midgett, M. Law, O. E. Semonin, R. J. Ellingson, A. J. Nozik, Nano Lett. 2009, 9, 836.
- [247] M. H. Zarghami, Y. Liu, M. Gibbs, E. Gebremichael, C. Webster, M. Law, ACS Nano 2010, 4, 2475.
- [248] Y. Liu, M. Gibbs, J. Puthussery, S. Gaik, R. Ihly, H. W. Hillhouse, M. Law, Nano Lett. 2010, 10, 1960.
- [249] O. E. Semonin, J. M. Luther, S. Choi, H.-Y. Chen, J. Gao, A. J. Nozik, M. C. Beard, Science 2011, 334, 1530.
- [250] J. Jasieniak, M. Califano, S. E. Watkins, ACS Nano 2011, 5, 5888.
- [251] I. J. Kramer, E. H. Sargent, Chem. Rev. 2014, 114, 863.
- [252] W. U. Huynh, J. J. Dittmer, N. Teclemariam, D. J. Milliron, A. P. Alivisatos, K. W. J. Barnham, Phys. Rev. B 2003, 67, 115326.
- [253] N. C. Greenham, X. Peng, A. P. Alivisatos, Phys. Rev. B 1996, 54, 17628.
- [254] E. Arici, H. Hoppe, F. Schaffler, D. Meissner, M. A. Malik, N. S. Sariciftci, Thin Solid Films 2004, 451, 612.
- [255] A. Maria, P. W. Cyr, E. J. D. Klern, L. Levina, E. H. Sargent, Appl. Phys. Lett. 2005, 87, 213112.
- [256] W. U. Huynh, J. J. Dittmer, A. P. Alivisatos, Science 2002, 295, 2425.
- [257] D. C. Oertel, M. G. Bawendi, A. C. Arango, V. Bulović, Appl. Phys. Lett. 2005, 87, 213505.
- [258] G. Konstantatos, J. Clifford, L. Levina, E. H. Sargent, Nat. Photonics 2007, 1, 531.
- [259] C. S. S. Sandeep, S. T. Cate, J. M. Schins, T. J. Savenije, Y. Liu, M. Law, S. Kinge, A. J. Houtepen, L. D. A. Siebbeles, Nat. Commun. 2013, 4, 2360.
- [260] M. Boberl, M. V. Kovalenko, S. Gamerith, E. J. W. List, W. Heiss, Adv. Mater. 2007, 19, 3574.
- [261] G. Konstantatos, L. Levina, J. Tang, E. H. Sargent, Nano Lett. 2008, 8, 4002.
- [262] A. Nag, M. V. Kovalenko, J.-S. Lee, W. Liu, B. Spokoyny, D. V. Talapin, J. Am. Chem. Soc. 2011, 133, 10612.
- [263] J. P. Clifford, G. Konstantatos, K. W. Johnston, S. Hoogland, L. Levina, E. H. Sargent, Nat. Nanotechnol. 2009, 4, 40.
- [264] A. Biebersdorf, R. Dietmuller, A. S. Susha, A. L. Rogach, S. K. Poznyak, D. V. Talapin, H. Weller, T. A. Klar, J. Feldmann, Nano Lett. 2006, 6,
- [265] K. Szendrei, F. Cordella, M. V. Kovalenko, M. Boberl, G. Hesser, M. Yorema, D. Jarzab, O. V. Mikhnenko, A. Gocalinska, M. Saba, F. Quochi, A. Mura, G. Bongiovanni, P. W. M. Blom, W. G. Heiss, M. A. Loi, Adv. Mater. 2009, 21, 683.
- [266] H.-Y. Chen, M. K. F. Lo, G. Yang, H. G. Monbouquette, Y. Yang, Nat. Nanotechnol. 2008, 3, 543.
- [267] T. Rauch, M. Böberl, S. F. Tedde, J. Fürst, M. V. Kovalenko, G. Hesser, U. Lemmer, W. Heiss, O. Hayden, Nat. Photonics 2009, 3, 332.



- [268] G. Konstantatos, M. Badioli, L. Gaudreau, J. Osmond, M. Bernechea, F. P. G. de Arquer, F. Gatti, F. H. L. Koppens, Nat. Nanotechnol. 2012, 73, 363.
- [269] B. A. Ridley, B. Nivi, J. M. Jacobson, Science 1999, 286, 746.
- [270] A. Dong, X. Ye, J. Chen, Y. Kang, T. Gordon, J. M. Kikkawa, C. B. Murray, J. Am. Chem. Soc. 2011, 133, 998.
- [271] E. Talgorn, E. Moysidou, R. D. Abellon, T. J. Savenije, A. Goossens, A. J. Houtepen, L. D. A. Siebbeles, J. Phys. Chem. C. 2010, 114, 3441.
- [272] S. Z. Bisri, C. Piliego, M. Yarema, W. Heiss, M. A. Loi, Adv. Mater. 2013, 25, 4309.
- [273] J.-S. Lee, M. V. Kovalenko, J. Huang, D. S. Chung, D. V. Talapin, Nat. Nanotechnol. 2011, 6, 348.
- [274] H. Zhang, J. Jang, W. Liu, D. V. Talapin, ACS Nano 2014, 8, 7359.
- [275] J.-H. Choi, S. J. Oh, Y. Lai, D. K. Kim, T. Zhao, A. T. Fafarman, B. T. Diroll, C. B. Murray, C. R. Kagan, ACS Nano 2013, 7, 8275.

- [276] D. K. Kim, Y. Lai, B. T. Diroll, C. B. Murray, C. R. Kagan, Nat. Commun. 2012, 3, 1216.
- [277] D. K. Kim, Y. Lai, T. R. Vemulkar, C. R. Kagan, ACS Nano 2011, 5, 10074.
- [278] I. Lokteva, S. Thiemann, F. Gannott, J. Zaumseil, Nanoscale 2013, 5, 4230.
- [279] X. Duan, Y. Huang, C. M. Lieber, Nano Lett. 2002, 2, 487.
- [280] Y. Zhou, S.-T. Han, X. Chen, F. Wang, Y.-B. Tang, V. A. L. Roy, Nat. Commun. 2014, 5, 4720.
- [281] J.-S. Lee, J. Cho, C. Lee, I. Kim, J. Park, Y.-M. Kim, H. Shin, J. Lee, F. Caruso, Nat. Nanotechnol. 2007, 2, 790.
- [282] V. Kannan, Y. S. Chae, CH. V. V. Ramana, D.-S. Ko, J. K. Rhee, J. Appl. Phys. 2011, 109, 086103.
- [283] H. I. Hanafi, S. Tiwari, I. Khan, IEEE Electron. Device Lett. 1996, 43, 1553.
- [284] S.-T. Han, Y. Zhou, Z.-X. Xu, L.-B. Huang, X.-B. Yang, V. A. L. Roy, Adv. Mater. 2012, 24, 3556.

1207